LA-UR--91-437

DE91 008580

TITLE THEORETICAL DESCRIPTIONS OF NEUTRON EMISSION IN FISSION

AUTHOR(S) David G. Madland, T-2

SUBMITTED TO The International Atomic Energy Agency, Vienna, for inclusion in the "Proceedings of the IAEA Consultants' Meeting on Nuclear Emission in the Fission Process," 22-24 October 1990, Vienna, Austria.

DISCLAIMER

Los Alamos Los Alamos National Laboratory
Los Alamos, New Mexico 87545

THEORETICAL DESCRIPTIONS OF NEUTRON EMISSION IN FISSION

David G. Madland
Theoretical Division, Los Alamos National Laboratory
Los Alamos, New Mexico 87545, USA

ABSTRACT

Brief descriptions are given of the observables in neutron emission in fission together with early theoretical representations of two of these observables, namely, the prompt fission neutron spectrum N(E) and the average prompt neutron multiplicity $\bar{\nu}_p$. This is followed by summaries, together with examples, of modern approaches to the calculation of these two quantities. Here, emphasis is placed upon the predictability and accuracy of the new approaches. In particular, the dependencies of N(E) and $\bar{\nu}_p$ upon the fissioning nucleus and its excitation energy are discussed. Then, recent work in multiple-chance fission and other recent work involving new measurements are presented and discussed. Following this, some properties of fission fragments are mentioned that must be better known and better understood in order to calculate N(E) and $\bar{\nu}_p$ with higher accuracy than is currently possible. In conclusion, some measurements are recommended for the purpose of benchmarking *simultaneous* calculations of neutron emission *and* gamma emission in fission.

I. INTRODUCTION AND EARLY REPRESENTATIONS

Neutron emission in fission can be described in terms of several experimental observables. These include the following:

- neutron emission times during the fission process (in principle),
- the energy spectrum of prompt fission neutrons N(E), where E is the laboratory energy of the emitted neutron and "prompt" refers to neutron emission prior to the onset of fission-fragment β-decay processes,
- the average number (multiplicity) of prompt neutrons emitted per fission $\bar{\nu}_p$,
- the various components of N(E) and $\bar{\nu}_p$ for fixed values of the fission-fragment total kinetic energy and/or fission-fragment mass number and/or neutron emission angle,
- the prompt fission neutron multiplicity distribution P(ν),
- the correlations and/or anti-correlations in neutron emission from complementary fragments,

- the energy spectrum of pre-fission neutrons $\phi(E)$ emitted prior to fission in multiple-chance fission,
- scission neutrons,
- neutron emission in ternary fission, and
- neutron emission from *accelerating* fragments in contrast to neutron emission from *fully accelerated* fragments.

While this list is not exhaustive, it does include most of the types of neutron emission measurements that have been performed or attempted. In this paper, the second and third items, the prompt fission neutron spectrum N(E) and the average prompt neutron multiplicity $\bar{\nu}_p$, will be discussed for both spontaneous and neutron-induced fission.

Two early representations of the prompt fission neutron spectrum, which are still used today, are the Maxwellian and Watt spectrum representations, with parameters that are adjusted to optimally reproduce the experimental spectrum for a given fissioning system. The Maxwellian spectrum is given by

$$N(E) = (2/\pi^{1/2} T_M^{3/2}) E^{1/2} \exp(-E/T_M) , \qquad (1)$$

where the single (temperature) parameter appearing, T_M, is related to the average energy of the spectrum <E> by

$$\langle E \rangle = (3/2)T_M . \qquad (2)$$

The Maxwellian spectrum neglects the distribution of fission-fragment excitation energy, the energy dependence of the inverse process of compound nucleus formation, and the center-of-mass motion of the fragments from which the neutrons are emitted. Thus, the single temperature parameter T_M must simultaneously account for all of these physical effects. Accordingly, there is no predictive power in a Maxwellian approach.

The two-parameter Watt spectrum[1] consists of a center-of-mass Maxwellian spectrum that has been transformed[2] to the laboratory system, for an average fission fragment moving with an average kinetic energy per nucleon E_f. This spectrum is given by

$$N(E) = \frac{\exp(-E_f/T_W)}{(\pi E_f T_W)^{1/2}} \exp(-E/T_W) \sinh[2(E_f E)^{1/2}/T_W] , \qquad (3)$$

where E_f and the Watt temperature T_W are related to the average energy of the spectrum <E> by

$$<E> = E_f + (3/2)T_W . \qquad (4)$$

The Watt spectrum also neglects the distribution of fission-fragment excitation energy and the energy dependence of the inverse process of compound nucleus formation, but does account for the center-of-mass motion of an average fragment. However, for spontaneous and low energy neutron-induced ($E_n < 15$ MeV) fission, the concept of an average fragment is usually not a good one because there are ordinarily two average fragments due to the double-humped fragment mass distribution. For these reasons, the Watt spectrum, although it is more physical than the Maxwellian spectrum, has little predictive power in most applications. [If one insists on using a Watt spectrum representation, the average of the separate Watt spectra for the light and heavy mass peaks should be taken to represent the total laboratory spectrum N(E). This amounts to a three-parameter representation, assuming the existence of statistical equilibrium between the nascent fragments.]

At the same time that these early representations were introduced for N(E), the average prompt neutron multiplicity $\bar{\nu}_p$ was modeled[3] by a simple polynomial (usually linear) in incident neutron energy E_n, for each fissioning system considered: $\bar{\nu}_p = \nu_o + \alpha E_n$, and again, the parameters appearing were, and are, adjusted to optimally reproduce the experimental average multiplicity.

To summarize, it is clear that one of the approaches described above can be used to predict N(E) and/or $\bar{\nu}_p(E_n)$ for a different fissioning nucleus or for a different excitation energy from what has been experimentally measured. Therefore, in Sec. II three modern approaches to the calculation of N(E) and $\bar{\nu}_p$ are described and examples given. More recent work with these approaches is described in Secs. III and IV, and some conclusions and recommendations are presented in Sec. V.

II. MODERN APPROACHES TO THE CALCULATION OF N(E) AND $\bar{\nu}_p$

In recent years three new theoretical approaches have evolved for the calculation of the prompt fission neutron spectrum N(E). These are the following:

- The Los Alamos approach,[4] begun in 1979, which is based upon standard nuclear evaporation theory[5] and simultaneously treats the average prompt neutron multiplicity $\bar{\nu}_p$. This approach emphasizes predictive capabilities while requiring minimal input. Refinements to this approach that treat the entire fission-fragment mass and charge distributions, instead of averages over their peak regions, have also been performed.[6-8]

- The Dresden approach,[9] begun in 1982, which is also based upon standard nuclear evaporation theory,[5] but accounts explicitly for neutron cascade emission. This approach emphasizes a complete description, requiring a substantial amount of experimental information. The Dresden group has also employed the Los Alamos approach including the refinements mentioned above.[6,10]

- The Hauser-Feshbach statistical model approach, which is based upon Hauser-Feshbach theory[11] and accounts explicitly for the competition between neutron emission and gamma-ray emission in a given fission fragment. This approach, if properly applied, accounts for the influence of angular momentum on neutron and gamma-ray emission, whereas the Los Alamos and Dresden approaches do not. Accordingly, the Hauser-Feshbach approach may, ultimately, become the best theoretical approach.

II.A. Summary of Los Alamos Model.

The original Los Alamos model[4] addresses both neutron-induced and spontaneous fission and accounts for the physical effects of

(1) the distribution of fission-fragment excitation energy,
(2) the energy dependence of the inverse process of compound nucleus formation,
(3) the center-of-mass motion of the fission fragments, and
(4) multiple-chance fission at high incident neutron energy.

In particular, to simulate the initial distribution of fission-fragment excitation energy and subsequent cooling as neutrons are emitted, a triangular approximation to the corresponding fission-fragment residual nuclear temperature distribution is used. This approximation, based upon the observations of Terrell [12] is given by

$$P(T) = \begin{cases} 2T/T_m^2 & T \le T_m \\ 0 & T > T_m \end{cases} , \qquad (5)$$

where the maximum temperature T_m is related to the initial total average fission-fragment excitation energy $<E^*>$ by

$$T_m = (<E^*>/a)^{1/2} , \qquad (6)$$

and where a is the nuclear level density parameter. In Eq. (6), the initial total average fission-fragment excitation energy is given by

$$<E^*> = <E_r> + E_n + B_n - <E_f^{tot}> , \qquad (7)$$

where $<E_r>$ is the average energy release in fission, B_n and E_n are the separation and kinetic energies of the neutron inducing fission (set to zero for spontaneous fission), and $<E_f^{tot}>$ is the total average fission-fragment kinetic energy. These quantities are either known or can be calculated.

The energy dependence of the inverse process is treated in the center-of-mass frame by calculating the compound nucleus formation cross section $\sigma_c(\varepsilon)$ for the inverse process using an optical-model potential with explicit isospin dependence so as to describe (neutron rich) fission fragments more correctly. It is the *shape of* $\sigma_c(\varepsilon)$ with ε that affects N(E).

The values of the average kinetic energy per nucleon of the average light fragment A_L and average heavy fragment A_H are obtained using momentum conservation and are given by

$$E_f^L = (A_H/A_L)(<E_f^{tot}>/A) ,$$

$$E_f^H = (A_L/A_H)(<E_f^{tot}>/A) , \qquad (8)$$

where A is the mass number of the fissioning nucleus.

With the inclusion of these physical effects, the prompt fission neutron spectrum in the laboratory system is given by

$$N(E) = \frac{1}{2}\left[N(E,E_f^L,\sigma_c^L) + N(E,E_f^H,\sigma_c^H)\right] , \qquad (9)$$

where

$$N(E,E_f,\sigma_c) = \frac{1}{2\sqrt{E_f}\,T_m^2} \int_{(\sqrt{E}-\sqrt{E_f})^2}^{(\sqrt{E}+\sqrt{E_f})^2} \sigma_c(\varepsilon)\sqrt{\varepsilon}\, d\varepsilon \int_0^{T_m} k(T)\, T \exp(-\varepsilon/T)\, dT . \qquad (10)$$

In this equation, ε is the center-of-mass neutron energy and the temperature-dependent normalization k(T) is given by

$$k(T) = \left[\int_0^\infty \sigma_c(\varepsilon)\,\varepsilon \exp(-\varepsilon/T)\, d\varepsilon\right]^{-1} . \qquad (11)$$

If $\sigma_c(\varepsilon)$ is constant, Eq. (10) reduces to the closed form expression

$$N(E,E_f) = \frac{1}{3(E_f T_m)^{1/2}}\left[u_2^{3/2}E_1(u_2) - u_1^{3/2}E_1(u_1) + \gamma(\tfrac{3}{2},u_2) - \gamma(\tfrac{3}{2},u_1)\right] , \qquad (12)$$

where

$$u_1 = (\sqrt{E} - \sqrt{E_f})^2/T_m ,$$

$$u_2 = (\sqrt{E} + \sqrt{E_f})^2/T_m ,$$

$E_1(x)$ is the exponential integral function, and

$\gamma(a,x)$ is the incomplete gamma function.

Similarly, the average prompt fission neutron multiplicity $\bar{\nu}_p$ is obtained from considerations of energy conservation and is given by

$$\bar{\nu}_p = \frac{\langle E^* \rangle - \langle E_\gamma^{tot} \rangle}{\langle S_n \rangle + \langle \varepsilon \rangle} , \qquad (13)$$

where $\langle E_\gamma^{tot} \rangle$ is the total average prompt gamma-ray energy, $\langle S_n \rangle$ is the average fission-fragment neutron separation energy, and $\langle \varepsilon \rangle$ is the average center-of-mass energy of the emitted neutrons.

There are two specific connections between N(E) and $\bar{\nu}_p$ that are worth noting. The first is that the maximum temperature T_m appearing as one of three parameters in N(E) also appears in $\bar{\nu}_p$ as T_m^2, through Eq. (6). The second is that the average center-of-mass neutron energy $\langle \varepsilon \rangle$ appearing in $\bar{\nu}_p$ is also the first moment of the center-of-mass spectrum $\phi(\varepsilon)$ corresponding to the laboratory spectrum N(E). These two connections are very important because they mean that if one has experimental information on either N(E) or $\bar{\nu}_p$ for a given fissioning system, then that information can be used as a constraint in the calculation of the other, unmeasured, observable.

If the complete fission-fragment mass and charge distributions are treated, instead of averages over their peak regions, Eq. (9) becomes

$$N(E) = \sum_A \frac{\bar{\nu}(A)}{\bar{\nu}_{tot}} Y(A) \sum_Z P(Z)\, N\left[E, E_f(A), \sigma_c(Z,A), T_m(Z,A) \right] , \qquad (14)$$

where (A,Z) are fragment mass and charge numbers,

$\bar{\nu}(A)$ is the average prompt neutron multiplicity for each fragment mass,

$Y(A)$ is the fragment mass yield,

$\bar{\nu}_{tot} = \sum_A Y(A)\, \bar{\nu}(A)$ is the total average prompt neutron multiplicity ,

$P(Z)$ is the fragment charge distribution,

and $E_f(A)$ and $T_m(Z,A)$ are calculated as in Eqs. (8) and (6), respectively, but without the use of any averaged quantities [see Ref. 7]. Similarly, if experimental values for $\bar{\nu}(A)$ do not exist, they are calculated as in Eq. (13), but without the use of corresponding averaged quantities.

Examples of calculations performed using the original Los Alamos model are shown in Figs. 1-7. The numerical details and evaluation of the constants appearing in these calculations are found in Ref. 4 so they are not repeated here. First, comparisons of the Los Alamos spectrum for a constant cross section to Maxwellian and Watt spectra for the same fissioning system are shown in Figs. 1 and 2. The first moments (average laboratory neutron energies) of the three spectra have been constrained to be identical by determining the Maxwellian and Watt temperatures, T_M and T_W, in terms of the physically

based value of T_m. Using this basis for comparison, the Los Alamos spectrum lies between the Maxwellian and Watt spectra. The fact that T_M includes the effects of fragment motion is evident in Fig. 2, where the tail of the Maxwellian spectrum is clearly too hard due to the overly large value of T_M. The converse is true for the tail of the Watt spectrum, which is too soft because T_W is less than T_m.

The dependence of N(E) on the fissioning nucleus and its excitation energy is shown for the constant cross section Los Alamos model in Figs. 3 and 4. Figure 3 shows how the spectrum increases at high energy and decreases at low energy as the mass and charge of the fissioning nucleus increases, for thermal-neutron-induced fission. Thus, $\langle E_r \rangle$ is increasing faster with the mass of the fissioning nucleus than $\langle E_f^{tot} \rangle$ is increasing with the charge of the fissioning nucleus [see Eqs. (6) and (7)]. Similarly, Fig. 4 shows how the spectrum increases at high energy and decreases at low energy as the kinetic energy of the incident neutron increases, for the first-chance fission of ^{235}U.

Figures 5 and 6 compare both the exact and approximate versions of the Los Alamos spectrum with experimental data. Clearly, there is a preference for the exact energy-dependent cross-section calculation, although both agree well with the experiment. Thus, given the quality of the experimental data, the Los Alamos exact spectrum given by Eqs. (9) and (10) is to be used when high accuracy is required. In such cases, the energy dependence of the inverse process of compound nucleus formation cannot be ignored.

Turning to the calculation of the average prompt neutron multiplicity $\bar{\nu}_p$ using the Los Alamos model, Fig. 7 shows a comparison of calculated and experimental values of $\bar{\nu}_p$ for the neutron-induced fission of ^{235}U. The agreement is better than 1% at energies below 1 MeV and at 6 MeV. In the region from ~ 1.5 to 5.5 MeV, however, the experimental values are somewhat less than the calculated values, ~ 3% differences at 4.5 MeV. Nevertheless, the agreement between experiment and calculation is quite good, given the approximations implied by the use of averaged quantities in Eq. (13).

A comparison of the original and (preliminary) refined Los Alamos models, corresponding to Eqs. (9) and (10) and Eqs. (14) and (10), respectively, is shown in Fig. 8 for the spontaneous fission of ^{252}Cf. The refined calculation agrees even better with experiment than does the original calculation [see Refs. 7-8], but there is still room for further improvement. This is presumably accomplished by increasing the number of calculated fragments from 28 (two fragments every sixth mass number) to say, 56 (two fragments every third mass number), or perhaps even more. This work is currently in progress.

II.B. Summary of Dresden Model.

The Dresden model,[9] currently known as the Complex Cascade Evaporation Model, accounts for the physical effects of

(1) the distribution of fission-fragment excitation energy in each step of the cascade evaporation of neutrons,
(2) the energy dependence of the inverse process of compound nucleus formation,
(3) the center-of-mass motion of the fission fragments,
(4) the anisotropy of the center-of-mass neutron spectrum,
(5) the complete fission-fragment mass and kinetic energy distributions, and
(6) semi-empirical fission-fragment nuclear level densities.

With knowledge of the above physical effects in sufficient detail, the prompt fission neutron spectrum in the laboratory system is given by

$$N(E) = \sum_{A} \int P(A,TKE)\, N(E,A,TKE)\, dTKE \quad , \tag{15}$$

where P(A,TKE) is the normalized fission-fragment mass distribution for a fixed value of the total fission-fragment kinetic energy TKE, and N(E,A,TKE) is the laboratory spectrum for fixed fragment mass A and fixed TKE. The sum and integral are over all contributing fragment mass numbers and total kinetic energies, respectively. The fragment spectrum N(E,A,TKE) is given by

$$N(E,A,TKE) = \int_{(\sqrt{E}-\sqrt{E_f})^2}^{(\sqrt{E}+\sqrt{E_f})^2} \frac{\phi(\varepsilon,A,TKE)}{4\sqrt{\varepsilon E_f}} \left\{ \frac{1 + b\,[(E - E_f - \varepsilon)^2/4\varepsilon E_f]}{[1 + (b/3)]} \right\} d\varepsilon \quad , \tag{16}$$

where E_f is the kinetic energy per nucleon of the fragment, b is the anistropy coefficient, ε is the center-of-mass neutron energy, and $\phi(\varepsilon,A,TKE)$ is the center-of-mass spectrum for fixed fragment mass and fixed TKE, given by

$$\phi(\varepsilon,A,TKE) = \sum_i \int_{B_i}^{\infty} \phi_i(\varepsilon,E^*,A-i)\, P_i\,(E^*,A,TKE)\, dE^* \quad . \qquad (17)$$

In this equation, the sum is over the steps i of the cascade while the integral is over the fragment excitation energy E^*, and B_i is the neutron binding energy in a fragment that has emitted i neutrons. Also, $P_i\,(E^*,A,TKE)$ is the excitation energy distribution *before* step i and is expressed in terms of P_{i-1} and, ultimately, P_0, which is assumed Gaussian. Finally, $\phi(\varepsilon,E^*,A)$ is the Weisskopf[5] center-of-mass neutron energy spectrum for fixed E^* and A, given by

$$\phi(\varepsilon,E^*,A) = C\,\sigma_c(\varepsilon,A-1)\,\varepsilon\,\rho(E^* - B_n - \varepsilon, A-1) \quad , \qquad (18)$$

where ρ is the level density of the residual nucleus for zero angular momentum states and C is the normalization constant.

Examples of calculations performed using the Dresden model are shown in Figs. 9 and 10 for the spontaneous fission of ^{252}Cf. The numerical details and evaluation of the constants appearing in these calculations are found in Refs. 13 and 14 so they are not repeated here. The reality of anisotropy effects in the prompt fission neutron spectrum is demonstrated in Fig. 9 where recent experimental data for polar and equatorial emission, and calculations using the Dresden model with an anisotropy coefficient $b = 0.1$, agree well with each other. The experimental and calculated spectra for the same fissioning system, but integrated over all angles of neutron emission, are shown in Fig. 10 as deviations from a Maxwellian spectrum. Again, the Dresden model (CEM), solid curve for $b = 0.1$ ($\beta = 0.1$), yields quite good agreement with experiment, especially at the low energy end of the spectrum. Clearly, the anisotropy of the center-of-mass spectrum must be taken into account to obtain the most realistic representation of the experimental spectrum.

The Dresden group has also employed[6,10] the Los Alamos model and has refined it (GMNM model) to include dependence on fragment mass and center-of-mass emission angle.[15]

II.C. Summary of Hauser-Feshbach Approach.

This approach consists of Hauser-Feshbach statistical model calculations of the de-excitation of representative nuclei of the fission-fragment mass and charge distributions.

This model applied to fission fragments accounts for the physical effects included in the Los Alamos and Dresden models and, *in addition*, accounts for

(1) Neutron and gamma-ray *competition* in the de-excitation of a given fission fragment,
(2) neutron transmission coefficients T_{lj} from an optical-model potential for each fragment considered [for each value of ε, these T_{lj} are essentially the angular momentum decomposition of the $\sigma_c(\varepsilon)$ used in the Los Alamos and Dresden models],
(3) gamma-ray transmission coefficients T_γ for each fragment considered, and
(4) the angular momentum distribution P(J) for each fragment considered.

A detailed description of the Hauser-Feshbach formalism for de-excitation of fission fragments is not presented here, due to space limitations. Crucial aspects of such calculations, however, include fragment nuclear level densities, initial excitation energy and angular momentum distributions, neutron optical-model potentials for fragments, and the partition of available excitation energies between light and heavy fragments. These subjects are discussed by Browne and Dietrich,[16] who performed a H-F calculation of the neutron spectrum N(E) for the ^{252}Cf(sf) reaction. Their results are compared with two experimental spectra (that were available in 1974) in Fig. 11. Gerasimenko and Rubchenya[17-18] have also performed H-F calculations of N(E), for the same ^{252}Cf(sf) reaction, beginning in 1980. They consider 18 representative fission fragments, and use a Fermi-gas level density and a Gaussian distribution of initial excitation energy, to obtain the total spectrum shown in good agreement with experiment in Fig. 12. They obtain even better agreement when including a center-of-mass anisotropy coefficient of b = 0.15, although this effect is still under study.[18]

More recent H-F calculations have been performed by Seeliger *et al.*[22], again, for the ^{252}Cf(sf) prompt neutron spectrum N(E). In these calculations, shown in Figs. 13 and 14, good agreement is obtained with evaluation and experiment. In particular, for the right value of a "scaling factor" on the gamma-emission width, the laboratory neutron energy spectrum and neutron total angular distribution are well reproduced. On the other hand, calculational difficulties remain with the average center-of-mass neutron emission energy as a function of fragment mass. This work is continuing.

III. RECENT WORK ON MULTIPLE-CHANCE FISSION

Two examples of recent work on the effects of neutron-induced multiple-chance fission upon the prompt fission neutron spectrum N(E) and average prompt neutron multiplicity $\bar{\nu}_p$ are discussed in this section. The major physical effect here is that when the incident neutron energy is sufficiently high (above the neutron binding energy, say), then two or more reaction channels resulting in fission can be open *simultaneously*. For example, the first-chance fission (n,f) reaction in competition with the second-chance fission (n,n'f) reaction. The *competition* between the open fission channels affects the observables N(E) and $\bar{\nu}_p$.

III.A. Neutron-Induced Multiple-Chance Fission of ^{235}U.

The Los Alamos model has been used to calculate the neutron-induced multiple-chance fission neutron spectrum and average multiplicity for ^{235}U up through third-chance fission. The exact energy-dependent spectra, given by Eqs. (9)-(11), together with evaporation spectra $\phi_j(E,\sigma_c)$ to describe neutron emission prior to fission, are combined in proportion to multiple-chance fission probabilities $P^A_{f_i}$ and average prompt neutron multiplicities $\bar{\nu}_{p_i}$ for the fissioning nuclei involved. This yields the total prompt fission neutron spectrum due to first-, second-, and third-chance fission events in the laboratory system:

$$N(E) = \left\{ P^A_{f_1} \bar{\nu}_{p_1} N_1(E) + P^A_{f_2} [\phi_1(E) + \bar{\nu}_{p_2} N_2(E)] + P^A_{f_3} [\phi_1(E) + \phi_2(E) + \bar{\nu}_{p_3} N_3(E)] \right\} / \left[P^A_{f_1} \bar{\nu}_{p_1} + P^A_{f_2} (1 + \bar{\nu}_{p_2}) + P^A_{f_3} (2 + \bar{\nu}_{p_3}) \right], \quad (19)$$

where the index "i" on P^A_f and $\bar{\nu}_p$ refers to first-, second-, or third-chance fission and the index "j" on ϕ refers to the corresponding neutron evaporation spectra prior to fission. [Note that these "ϕ" are different from the "ϕ" of the Dresden model described above.]

Similarly, the total average prompt neutron multiplicity due to first-, second-, and third-chance fission events is given by

$$\bar{\nu}_p = \left[P^A_{f_1} \bar{\nu}_{p_1} + P^A_{f_2}(1 + \bar{\nu}_{p_2}) + P^A_{f_3}(2 + \bar{\nu}_{p_3}) \right] / (P^A_{f_1} + P^A_{f_2} + P^A_{f_3}) , \qquad (20)$$

where the indices have the same meaning as in Eq. (19).

The evaluation of Eq. (19) and Eq. (20) as a function of incident neutron energy E_n leads to the prompt fission neutron spectrum matrix $N(E,E_n)$ and the average prompt neutron multiplicity vector $\bar{\nu}_p(E_n)$. These are shown for n + ^{235}U in Figs. 15 and 16 for $N(E,E_n)$, and in Fig. 17 for $\bar{\nu}_p(E_n)$. Detailed features of these calculations are discussed in Ref. 4 and in Ref. 7. Figures 15 and 16 clearly illustrate the dependence of the matrix $N(E,E_n)$ upon the incident neutron energy E_n. In particular, the partition of the total available excitation energy into neutron emission prior to fission and neutron emission from fission fragments leads to suggestions of a *staircase effect* in the peak regions of the matrix and an *oscillatory effect* in the tail regions of the matrix. The staircase effect is due largely to the pre-fission evaporation neutrons while the oscillatory effect is due largely to the c·-currence of cooler fission fragments following the emission of a neutron, or two neutrons, prior to fission. Figure 17 illustrates the calculated vector $\bar{\nu}_p(E_n)$, under the assumptions of multiple-chance fission and first-chance fission only, in comparison with experiment. Surprisingly, there are only slight differences between the two calculations for the n + ^{235}U system. This means that the combined incident energy dependencies of the components of Eq. (20) and those of Eq. (13) are very similar, perhaps fortuitously so.

III.B. Neutron-Induced Multiple-Chance Fission of ^{232}Th.

The Dresden group has employed a refined version of the Los Alamos model (their GMNM model[6]) to calculate the neutron-induced multiple-chance fission neutron spectrum and average neutron multiplicity for ^{232}Th. The spectrum N(E) is calculated for E_n = 7.3 MeV, at which the Dresden group also measured the spectrum.[25] The average multiplicity is calculated[15] from threshold to 10 MeV. The calculations of these two observables then require inclusion of first- and second-chance fission effects from the standpoint of energetics. A comparison of the measured and calculated spectra is shown in Fig. 18, without illustration of first- and second-chance components, because the spectrum is "not influenced by pre-fission neutrons above 1 MeV." This implies that, for this case, multiple-chance fission effects are found to be negligible. On the other hand, the measured and calculated average neutron multiplicities, shown in Fig. 19, indicate the presence of second-chance fission effects just above 6 MeV and a very strong second-chance fission component at ~ 7 MeV. Comparing with the ^{235}U case for both observables, one sees that

N(E, 7 MeV) for ^{235}U, Fig. 16, shows a reasonably strong second-chance fission presence in sharp contrast to N(E, 7.3 MeV) for ^{232}Th, shown in Fig. 18, whereas the converse is true for $\bar{\nu}_p$ in the same energy region, as shown in Figs. 17 and 19. Although differences in both macroscopic and microscopic components of the respective potential energy surfaces, together with differences in the energetics, are responsible for this circumstance, it is nevertheless difficult to isolate a dominant cause. Clearly, there is a need for further studies in multiple-chance fission.

IV. OTHER RECENT WORK

In this section other recent work is presented on the calculation of the prompt fission neutron spectrum N(E). Some of these calculations are due to the completion of very recent measurements.

IV.A. N(E,θ) for ^{252}Cf(sf).

The Dresden group has applied the Los Alamos model to the calculation of the energy and angle spectrum, N(E,θ), for the ^{252}Cf(sf) reaction. To accomplish this, they have written a new computer code,[15] FINESSE, which is based upon a refined Los Alamos model (their GMNM model[6]). The calculated[15] spectrum is shown in the upper portion of Fig. 20 in comparison with smoothed experimental data[24] shown in the lower portion of the figure. The good overall agreement is a rather remarkable achievement, despite the reported strong sensitivity of the tail of the spectrum to the optical potential employed.

IV.B. N(E, 0.53 MeV) for the n + ^{235}U and n + ^{239}Pu Reactions.

Calculations for the identical fission reactions are compared here for the original Los Alamos model (Ref. 4, 1982) and the Los Alamos model refined by the Dresden group (Ref. 15, 1990). The experimental data for the n + ^{235}U and n + ^{239}Pu reactions, at E_n = 0.53 MeV, are those of Johansson and Holmqvist[26] and Johansson *et al.*,[27] respectively. The comparisons are shown in Figs. 21 and 22, wherein the calculations (and data) for the original Los Alamos model[4] are referenced to the constant cross-section calculation (Eqs. 9 and 12), while the calculations (and data) for the Los Alamos model refined[15] by the Dresden group are referenced to best-fit Maxwellian spectra. The figures show that the original Los Alamos model agrees better with the ^{235}U data, although the refined Los

Alamos model calculation is in reasonable agreement. On the other hand, neither calculation agrees well with the ^{239}Pu experiment. This means that the calculations are in error, or that the experimental data are suspect, or both. Clearly, existing ^{239}Pu data at other incident energies should be calculated as the first step in resolving this discrepancy.

IV.C. N(E, 0 MeV) for the n + ^{235}U Reaction.

A new measurement of the prompt fission neutron spectrum for the thermal-neutron-induced fission of ^{235}U has been reported by Wang *et al.*[28] in 1989. This spectrum was calculated[29] in 1983 using the Los Alamos model, Eqs. (9)-(11), and is identical to the thermal spectrum shown in Figs. 15 and 16. The comparison with the new data is shown in Figs. 23 and 24. Since the measurement occurred six years after the calculation, the comparison is certainly one without parameter adjustment. Although the agreement is reasonably good, the low energy ($E < \sim 1$ MeV) end of the spectrum is underpredicted. This may be further evidence for center-of-mass anisotropy, which is not included in the calculation.

IV.D. N(E, 2 MeV) for the n + ^{238}U Reaction.

A new measurement of the prompt fission neutron spectrum has also been reported[30] for 2-MeV neutrons incident on ^{238}U. The spectrum was calculated with the Los Alamos model, Eqs. (9)-(11), using input parameters, except the value of E_n, determined in 1982 (Ref. 4), and is compared with the new data of Baba *et al.*[30] in Figs. 25 and 26. Here also, the agreement is reasonably good, especially given that no parameter adjustments have been made. However, the constant cross-section version of the Los Alamos model, Eqs. (9) and (12), was also used to calculate this spectrum (JENDL-3) and is shown in Ref. 30 (Fig. 6). A comparison of the two different calculations clearly shows that, in this case, the energy-dependent cross section calculation is the preferred one. It should be noted here that an adjustment in the effective level density parameter of the JENDL-3 calculation would improve the agreement.

V. CONCLUSIONS AND RECOMMENDATIONS

It is concluded that prompt fission neutron spectra and average prompt neutron multiplicities can be calculated with reasonably good confidence

- for unmeasured as well as measured systems, and

- for spontaneous as well as neutron-induced fission.

A high-quality measurement of the prompt fission neutron spectrum matrix from neutron-induced multiple-chance fission, a fission coincidence measurement, would crucially test the already existing calculations for multiple-chance fission effects. This would undoubtedly lead to a better understanding of multiple-chance fission effects, especially in their competition.

The current limitations to calculating $N(E)$, $N(E,E_n)$, and $\bar{\nu}_p(E_n)$ with higher accuracy than is now possible include insufficient knowledge of

- excitation energy partition in fission,
- fission-fragment nuclear level densities,
- isospin dependence of global neutron optical-model potentials,
- fission-fragment ground-state masses (for the calculation of fission energy release),
- fission-fragment mass and charge distributions (as opposed to these distributions for fission products), and
- fission-fragment initial excitation energy and initial angular momentum distributions.

It is believed that, ultimately, the Hauser-Feshbach approach will probably yield the most accurate results in the calculation of $N(E)$, $N(E,E_n)$, and $\bar{\nu}_p(E_n)$. One of the reasons for this belief is that simultaneous calculation of neutron and gamma-ray competition is the best way to account for the available fission-fragment excitation energy. Another reason is the explicit treatment of each fragment pair in the calculation. To benchmark such calculations, it is recommended that the following measurements be performed with high accuracy and over the widest possible secondary energy range, if they do not already exist:

- The prompt fission neutron and gamma-ray spectra for the thermal-neutron-induced fission of ^{235}U (leading to compound nucleus spin/parity of 3^- and 4^- only), and

- the prompt fission neutron and gamma-ray spectra for the thermal-neutron-induced fission of ^{239}Pu (leading to compound nucleus spin/parity of 0^+ and 1^+ only).

It is clear that these measurements would, ideally, be performed on a fragment pair by fragment pair basis.

REFERENCES

1. B. E. Watt, Phys. Rev. **87**, 1037 (1952).

2. N. Feather, "Emission of Neutrons from Moving Fission Fragments," BM-148, British Mission (1942).

3. See, for example, F. Manero and V. A. Konshin, Atomic Energy Rev. **10**, 637 (1972).

4. D. G. Madland and J. R. Nix, Nucl. Sci. Eng. **81**, 213 (1982), and earlier references contained therein.

5. V. F. Weisskopf, Phys. Rev. **52**, 295 (1937).

6. H. Märten and D. Seeliger, Nucl. Sci. Eng. **93**, 370 (1986).

7. D. G. Madland, R. J. LaBauve, and J. R. Nix, *Proceedings of the IAEA Consultants' Meeting on the Physics of Neutron Emission in Fission, Mito, Japan, 1988*, H. D. Lemmel, Ed. [IAEA, INDC(NDS)-220, 1989], p. 259.

8. D. G. Madland, *Proceedings of the International Conference Nuclear Data for Science and Technology, Mito, Japan, 1988*, S. Igarasi, Ed. (Saikon Publishing, Tokyo, 1988), p. 759.

9. H. Märten and D. Seeliger, J. Phys. G **10**, 349 (1984), and earlier references contained therein.

10. H. Märten, A. Ruben, and D. Seeliger, *Proceedings of the IAEA Consultants' Meeting on the Physics of Neutron Emission in Fission, Mito, Japan, 1988*, H. D. Lemmel, Ed. [IAEA, INDC(NDS)-220, 1989], p. 245.

11. W. Hauser and H. Feshbach, Phys. Rev. **87**, 366 (1952).

12. J. Terrell, Phys. Rev. **113**, 527 (1959).

13. D. Seeliger, H. Märten, W. Neubert, and D. Richter, Sov. J. Nucl. Phys. **47**, 403 (1988).

14. H. Märten and D. Seeliger, *Proceedings of the Advisory Group Meeting on Nuclear Standard Reference Data, Geel, Belgium, 1984* (IAEA-TECDOC-335, Vienna, 1985), p. 255.

15. D. Seeliger, H. Märten, and A. Ruben, *Contributions to the Theory of Fission Neutron Emission* [INDC(GDR)-057, Vienna, 1990].

16. J. C. Browne and F. S. Dietrich, Phys. Rev. C. **10**, 2545 (1974).

17. B. F. Gerasimenko and V. A. Rubchenya, *Proceedings of the Advisory Group Meeting on Properties of Neutron Sources, Leningrad, USSR, 1986* (IAEA-TECDOC-410, Vienna, 1987), p. 208, and earlier references contained therein.

18. B. F. Gerasimenko and V. A. Rubchenya, *Proceedings of the IAEA Consultants' Meeting on the Physics of Neutron Emission in Fission, Mito, Japan, 1988*, H. D. Lemmel, Ed. [IAEA, INDC(NDS)-220, 1989], p. 283.

19. J. W. Meadows, Phys. Rev. **157**, 1076 (1967).

20. L. Green, J. A. Mitchell, and N. M. Steen, Nucl. Sci. Eng. **50**, 257 (1973).

21. O. Balenkov *et al.*, *"Proceedings of the IAEA Consultants' Meeting on the U-235 Fast-Neutron Fission Cross Section and the Cf-252 Fission Neutron Spectrum, Smolenice, Czechoslovakia, 1983*, H. D. Lemmel and D. E. Cullen, Eds. [IAEA, INDC(NDS)-146, 1983], p. 161.

22. D. Seeliger, *et al., Prompt Neutron Emission in Nuclear Fission* [INDC(GDR)-056/L, Vienna, 1989], p. 8.

23. W. Mannhart, *Proceedings of the Advisory Group Meeting on Properties of Neutron Sources, Leningrad, USSR, 1986* (IAEA-TECDOC-410, Vienna, 1987), p. 158.

24. H. Märten *et al.*, Nucl. Instr. Meth. **A264**, 375 (1988).

25. H. Märten *et al.*, *Proceedings of the IAEA Consultants' Meeting on the Physics of Neutron Emission in Fission, Mito, Japan, 1988*, H. D. Lemmel, Ed. [IAEA, INDC(NDS)-220, 1989], p. 169.

26. P. I. Johansson and B. Holmqvist, Nucl. Sci. Eng. **62**, 695 (1977).

27. P. I. Johansson *et al.*, *Proceedings of the Conference on Nuclear Cross Sections and Technology, Washington, DC, 1975* (NBS Special Publication 425, U.S. National Bureau of Standards, 1975) Vol. II, p. 572.

28. Wang Yufeng *et al.*, Chin. Jour. Nucl. Phys. **11**, 47 (1989).

29. D. G. Madland and J. R. Nix, *Proceedings of the NEANDC Specialists' Meeting on Yields and Decay Data of Fission Product Nuclides, Brookhaven National Laboratory, Upton, NY, 1983*, R. E. Chrien and T. W. Burrows, Eds. (BNL 51778, 1984), p. 423.

30. M. Baba *et al.*, J. Nucl. Sci. Technol. **27**, 601 (1990).

31. F. D. Becchetti, Jr. and G. W. Greenlees, Phys. Rev. **182**, 1190 (1969).

32. H. R. Bowman *et al.*, Phys. Rev. **126**, 2120 (1962).

FIGURE CAPTIONS

Fig. 1. Prompt fission neutron spectrum for the fission of ^{235}U induced by 0.53-MeV neutrons. The solid curve gives the Los Alamos spectrum calculated from Eqs. (9) and (12), the dashed curve gives the Watt spectrum calculated from Eq. (3), and the dot-dashed curve gives the Maxwellian spectrum calculated from Eq. (1). The average neutron energies of the three spectra are identical.

Fig. 2. Ratio of the Watt spectrum and the Maxwellian spectrum to the Los Alamos spectrum, corresponding to the curves shown in Fig. 1.

Fig. 3. Dependence of the prompt fission neutron spectrum on the fissioning nucleus, for thermal-neutron-induced fission, calculated using the Los Alamos model, Eqs. (9) and (12), for $\sigma_c(\varepsilon)$ = constant.

Fig. 4. Dependence of the prompt fission neutron spectrum on the kinetic energy of the incident neutron for the fission of ^{235}U, calculated using the Los Alamos model, Eqs. (9) and (12), for $\sigma_c(\varepsilon)$ = constant and assuming first-chance fission only.

Fig. 5. Prompt fission neutron spectrum for the fission of ^{235}U induced by 0.53-MeV neutrons. The dashed curve gives the Los Alamos spectrum calculated from Eqs. (9) and (12), for $\sigma_c(\varepsilon)$ = constant, whereas the solid curve gives the Los Alamos spectrum calculated from Eqs. (9)-(11), for $\sigma_c(\varepsilon)$ obtained using the optical-model potential of Becchetti and Greenlees (Ref. 31). The experimental data are those of Johansson and Holmqvist (Ref. 25).

Fig. 6. Ratio of the Los Alamos spectrum calculated using energy-dependent cross sections and the experimental spectrum to the Los Alamos spectrum calculated using a constant cross section, corresponding to the curves shown in Fig. 5.

Fig. 7. Average prompt neutron multiplicity as a function of the incident neutron energy for the neutron-induced fission of ^{235}U. The solid curve gives the Los Alamos multiplicity calculated with Eq. (13) using the optical-model potential of Becchetti and Greenlees (Ref. 31) to calculate the average center-of-mass energy $\langle\varepsilon\rangle$. The experimental data are listed in Ref. 4.

Fig. 8. Ratio of the original Los Alamos spectrum, based upon considerations of the *peaks* of the fission-fragment mass and charge distributions, and the (preliminary) refined Los Alamos spectrum, based on considerations of the *entire* fission-fragment mass and charge distributions, to a Maxwellian spectrum with T_M = 1.42 MeV. The nuclear level-density parameter is identical in both calculations.

Fig. 9. Prompt fission neutron spectra for the spontaneous fission of ^{252}Cf in the parallel (polar) and perpendicular (equatorial) directions with respect to the fission axis, calculated using the Dresden model (CEM), Eqs. (15)-(18), but prior to integration over angle. The experimental data are from Ref. 13 (closed circles) and Ref. 32 (crosses). [Figure is from Ref. 13.]

Fig. 10. Prompt fission neutron spectra for the spontaneous fission of ^{252}Cf shown as the deviation, in per cent, from a Maxwellian spectrum with T_M = 1.42 MeV. The solid curves are calculated using the Dresden model (CEM), Eqs. (15)-(18), for two values of the anisotropy coefficient b (β in the figure). Calculations are also shown for the Hauser-Feshbach (HFC) and Los Alamos (GMNM and MNM) models. The experimental data points are from the indicated laboratories, but with error deleted for clarity. [Figure is from Ref. 14.]

Fig. 11. Prompt fission neutron spectrum for the spontaneous fission of ^{252}Cf, calculated by Browne and Dietrich (Ref. 16) using the Hauser-Feshbach approach, together with experimental data from Meadows (Ref. 19) and Greene *et al.* (Ref. 20). [Figure is from Ref. 16.]

Fig. 12. Prompt fission neutron spectrum for the spontaneous fission of ^{252}Cf shown as the deviation, in per cent, from a Maxwellian spectrum with T_M = 1.42 MeV. The calculated spectrum using the Hauser-Feshbach approach has been obtained by Gerasimenko and Rubchenya (Ref. 17) and the experimental data are from Balenkov *et al.* (Ref. 21). [Figure is from Ref. 17.]

Fig. 13. Prompt fission neutron spectrum for the spontaneous fission of ^{252}Cf shown as the deviation, in per cent, from a Maxwellian spectrum with T_M = 1.42 MeV. The Hauser-Feshbach calculations of the spectra, performed by Seeliger *et al.* (Ref. 22) are shown for three values of a "scaling factor" on the gamma-emission width. The evaluated data are from Mannhart (Ref. 23). [Figure is from Ref. 22.]

Fig. 14. Neutron total angular distribution from the spontaneous fission of ^{252}Cf. The Hauser-Feshbach calculations of the angular distribution, performed by Seeliger *et al.* (Ref. 22) are shown for three values of a "scaling factor" on the gamma-emission width. The experimental data are from Märten *et al.* (Ref. 24). [Figure is from Ref. 22.]

Fig. 15. Prompt fission neutron spectrum matrix $N(E,E_n)$ for the neutron-induced fission of ^{235}U as a function of incident neutron energy E_n and emitted neutron energy E, and calculated using the Los Alamos model, Eqs. (9)-(11), and (19).

Fig. 16. Prompt fission neutron spectrum ratio matrix $R(E,E_n) = N(E,E_n)/N(E,0)$, corresponding to the matrix shown in Fig. 15.

Fig. 17. Average prompt neutron multiplicity for the neutron-induced fission of ^{235}U. The dashed curve gives the multiplicity calculated with Eq. (13) assuming first-chance fission, whereas the solid curve gives the multiplicity calculated with Eq. (20) assuming multiple-chance fission. In both cases, the optical-model potential of Becchetti and Greenlees (Ref. 31) is used to calculate the average center-of-mass energy $\langle\varepsilon\rangle$. The experimental data are listed in Ref. 4.

Fig. 18. Prompt fission neutron spectrum from the neutron-induced fission of ^{232}Th calculated, using the Dresden version (GMNM) of the Los Alamos model, and measured by Märten *et al.* (Ref. 25). [Figure is from Ref. 25.]

Fig. 19. Average prompt multiplicity as a function of the incident neutron energy for the neutron-induced fission of ^{232}Th. The solid curve gives the calculation (Ref. 15) using the Dresden version (GMNM) of the Los Alamos model. [Figure is from Ref. 15.]

Fig. 20. Prompt fission neutron spectrum energy and angle matrix $N(E,\theta)$ for the $^{252}Cf(sf)$ reaction, calculated (Ref. 15) using the Dresden version (GMNM) of the Los Alamos model (upper portion of figure), and compared with the smoothed experimental data of Märten *et al.* (Ref. 24) (lower portion of figure). [Figure is from Ref. 15.]

Fig. 21. (a) Prompt fission neutron spectrum for the fission of ^{235}U induced by 0.53-MeV neutrons. The solid curve gives the ratio of the Los Alamos spectrum calculated (Ref. 4) using energy-dependent cross sections and the experimental spectrum to the Los Alamos spectrum calculated using a constant cross section. The experimental data are those of Johansson and Holmqvist (Ref. 26). (b) Identical to (a) except that the calculation (Ref. 15) is the Dresden version (GMNM) of the Los Alamos model and the reference spectrum is the best-fit Maxwellian with T_M = 1.318 MeV.

Fig. 22. (a) Identical to Fig. 21(a) except for ^{239}Pu, and where the experimental data are those of Johansson *et al.* (Ref. 27). (b) Identical to Fig. 21(b) except for ^{239}Pu, and where the experimental data are those of Johansson *et al.* (Ref. 27).

Fig. 23. Prompt fission neutron spectrum for the fission of ^{235}U induced by thermal neutrons. The dashed curve gives the best-fit Maxwellian spectrum (T_M = 1.321 MeV) determined in Ref. 28, and the solid curve gives the Los Alamos spectrum calculated from Eqs. (9)-(11) for $\sigma_c(\varepsilon)$ obtained using the optical-model potential of Becchetti and Greenlees (Ref. 31). The experimental data are those of Wang *et al.* (Ref. 28).

Fig. 24. Ratio of the Los Alamos spectrum and the experimental spectrum to the best-fit Maxwellian spectrum, corresponding to the curves shown in Fig. 23.

Fig. 25. Prompt fission neutron spectrum for the fission of ^{238}U induced by 2-MeV neutrons. The dashed curve gives the best-fit Maxwellian (T_M = 1.24 MeV) determined in Ref. 30, and the solid curve gives the Los Alamos spectrum calculated from Eqs. (9)-(11) for $\sigma_c(\varepsilon)$ obtained using the optical-model potential of Becchetti and Greenlees (Ref. 31). The experimental data are those of Baba *et al.* (Ref. 30).

Ref. 26. Ratio of the Los Alamos spectrum and the experimental spectrum to the best-fit Maxwellian spectrum, corresponding to the curves shown in Fig. 25.

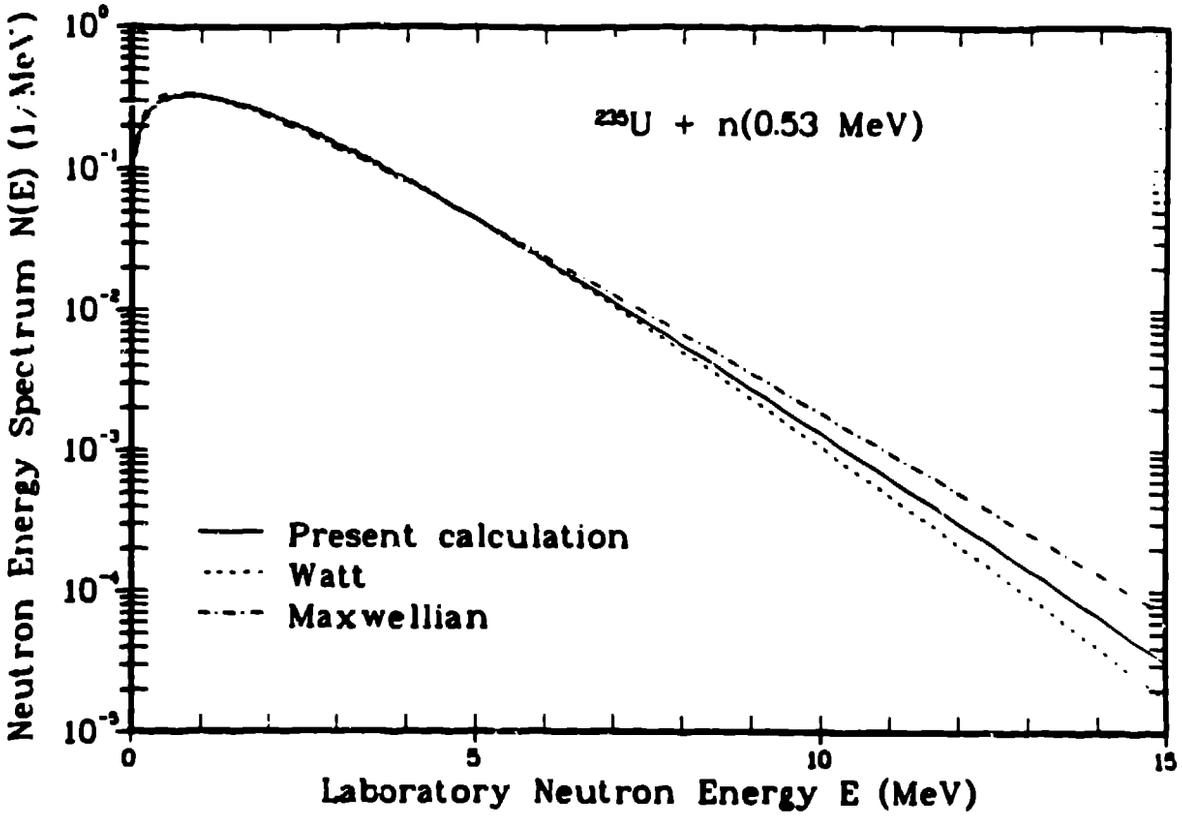
Neutron Energy Spectrum N(E) (1/MeV)
^{235}U + n(0.53 MeV)
Present calculation
Watt
Maxwellian
Laboratory Neutron Energy E (MeV)

Fig. 1.

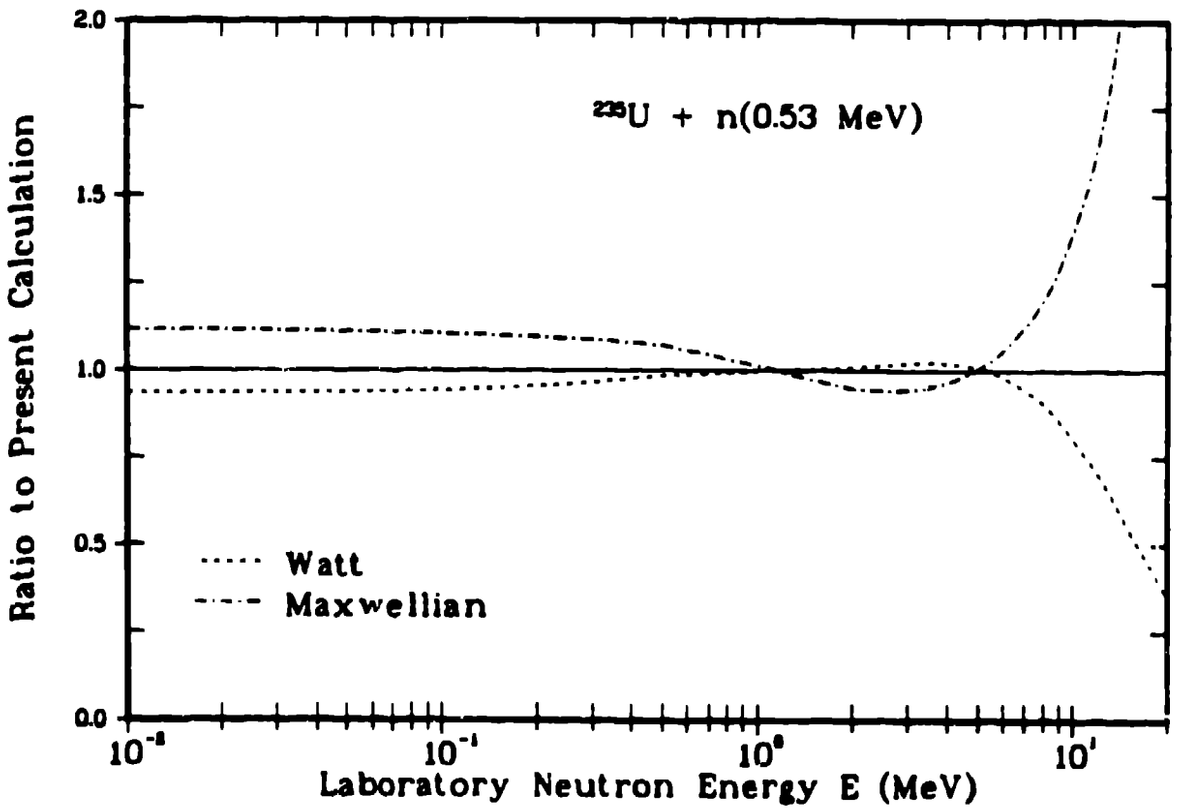
Ratio to Present Calculation
^{235}U + n(0.53 MeV)
Watt
Maxwellian
Laboratory Neutron Energy E (MeV)

Fig. 2.

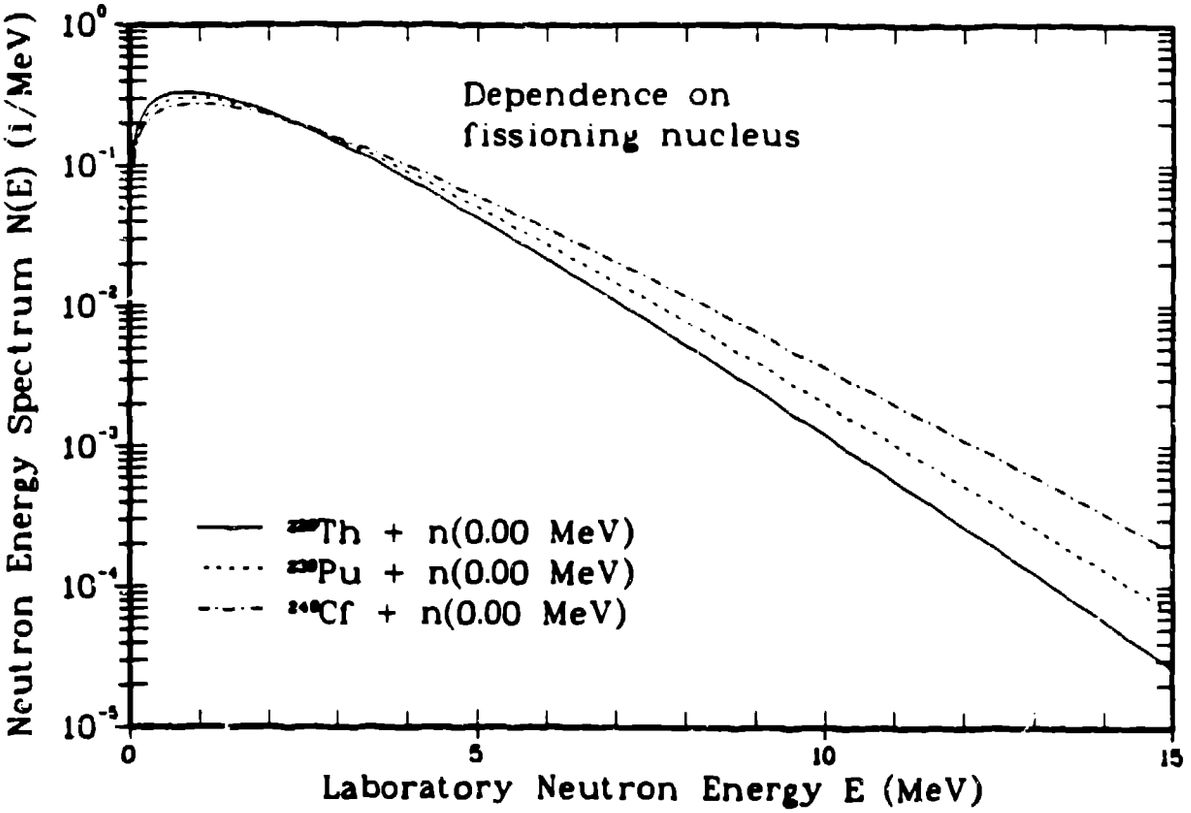
Dependence on
fissioning nucleus
^{232}Th + n(0.00 MeV)
^{239}Pu + n(0.00 MeV)
^{249}Cf + n(0.00 MeV)
Neutron Energy Spectrum N(E) (1/MeV)
Laboratory Neutron Energy E (MeV)
10^{0}
10^{-1}
10^{-2}
10^{-3}
10^{-4}
10^{-5}
0
5
10
15

Fig. 3.

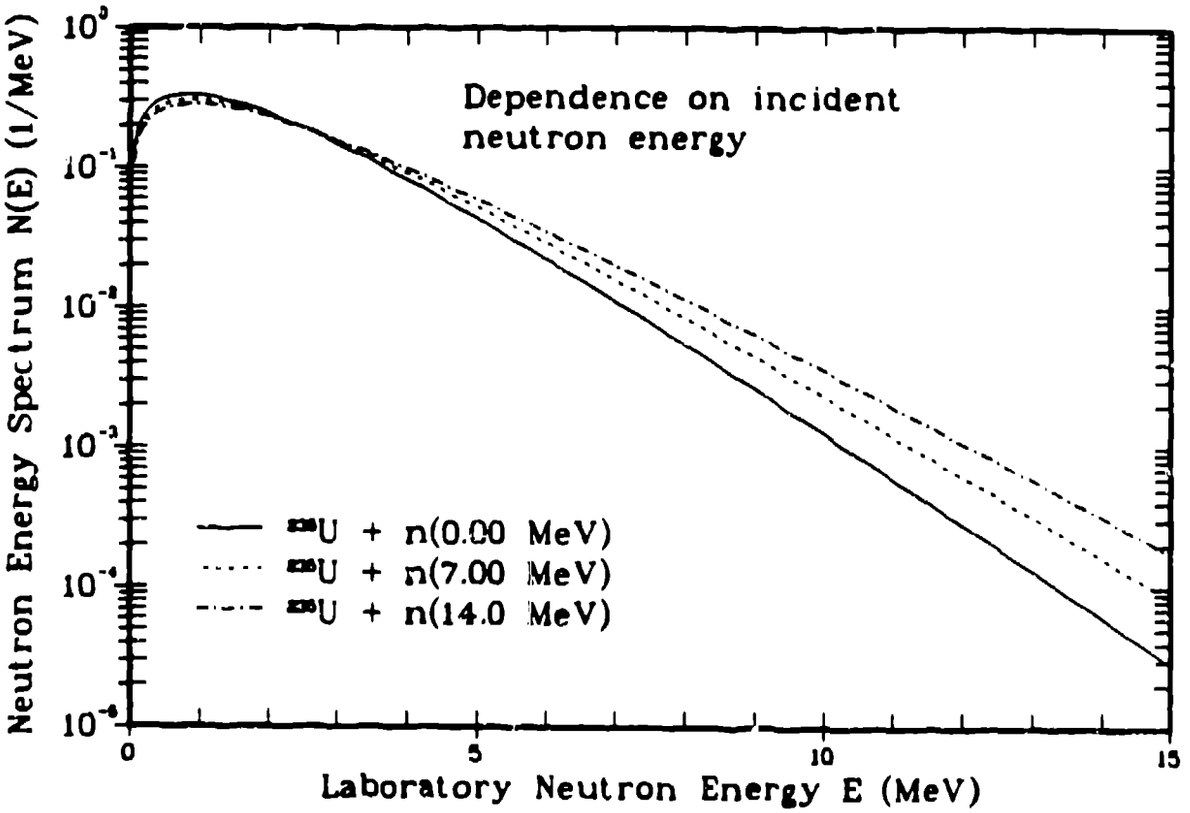
Dependence on incident
neutron energy
^{238}U + n(0.00 MeV)
^{238}U + n(7.00 MeV)
^{238}U + n(14.0 MeV)
Neutron Energy Spectrum N(E) (1/MeV)
Laboratory Neutron Energy E (MeV)
10^{0}
10^{-1}
10^{-2}
10^{-3}
10^{-4}
10^{-5}
0
5
10
15

Fig. 4.

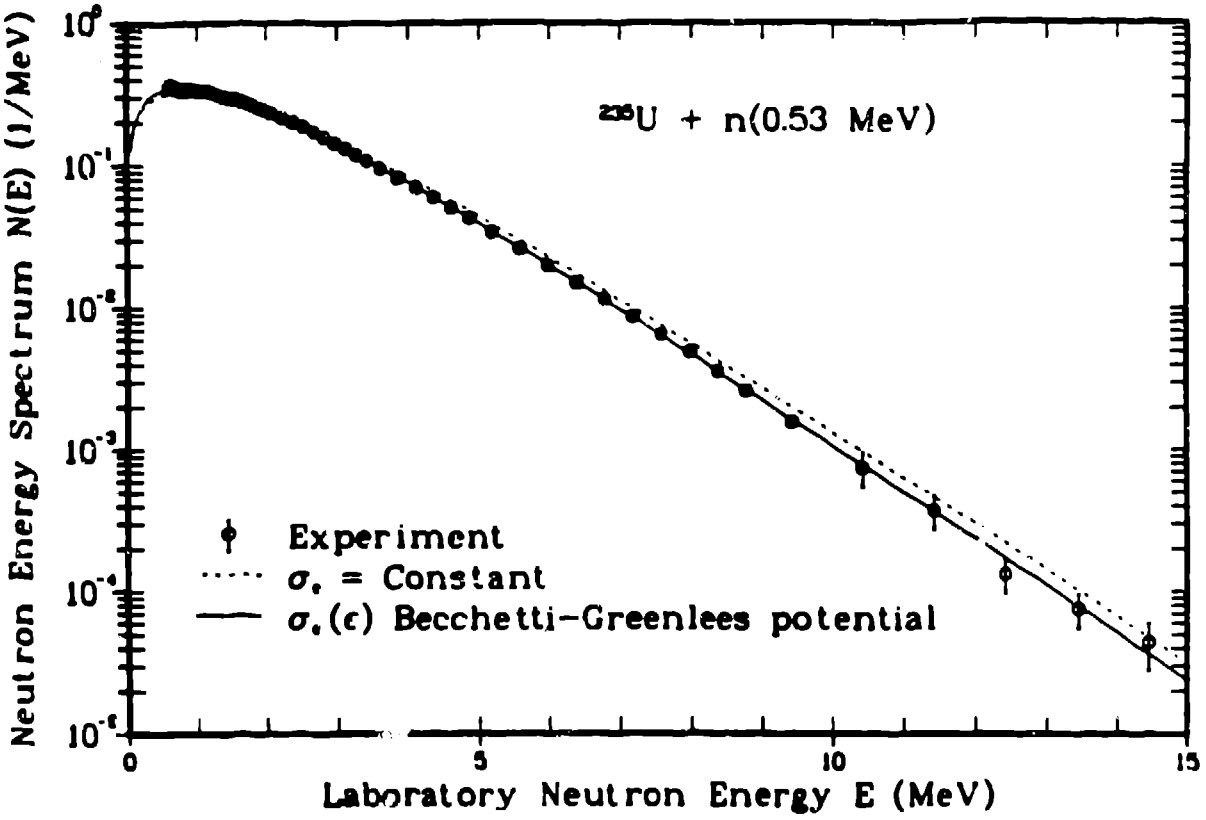
Neutron Energy Spectrum N(E) (1/MeV)
^{235}U + n(0.53 MeV)
Experiment
σ_c = Constant
$\sigma_c(\epsilon)$ Becchetti-Greenlees potential
Laboratory Neutron Energy E (MeV)

Fig. 5.

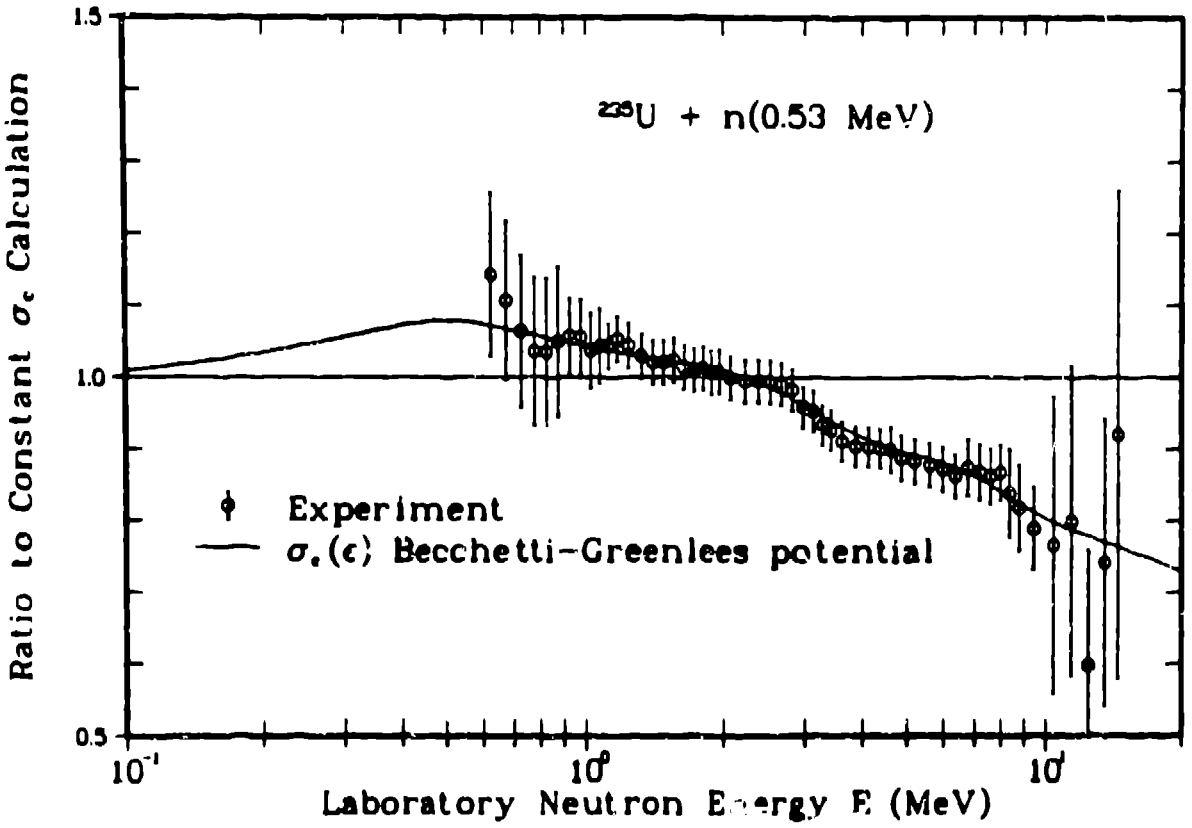
Ratio to Constant σ_c Calculation
^{235}U + n(0.53 MeV)
Experiment
$\sigma_c(\epsilon)$ Becchetti-Greenlees potential
Laboratory Neutron Energy E (MeV)

Fig. 6.

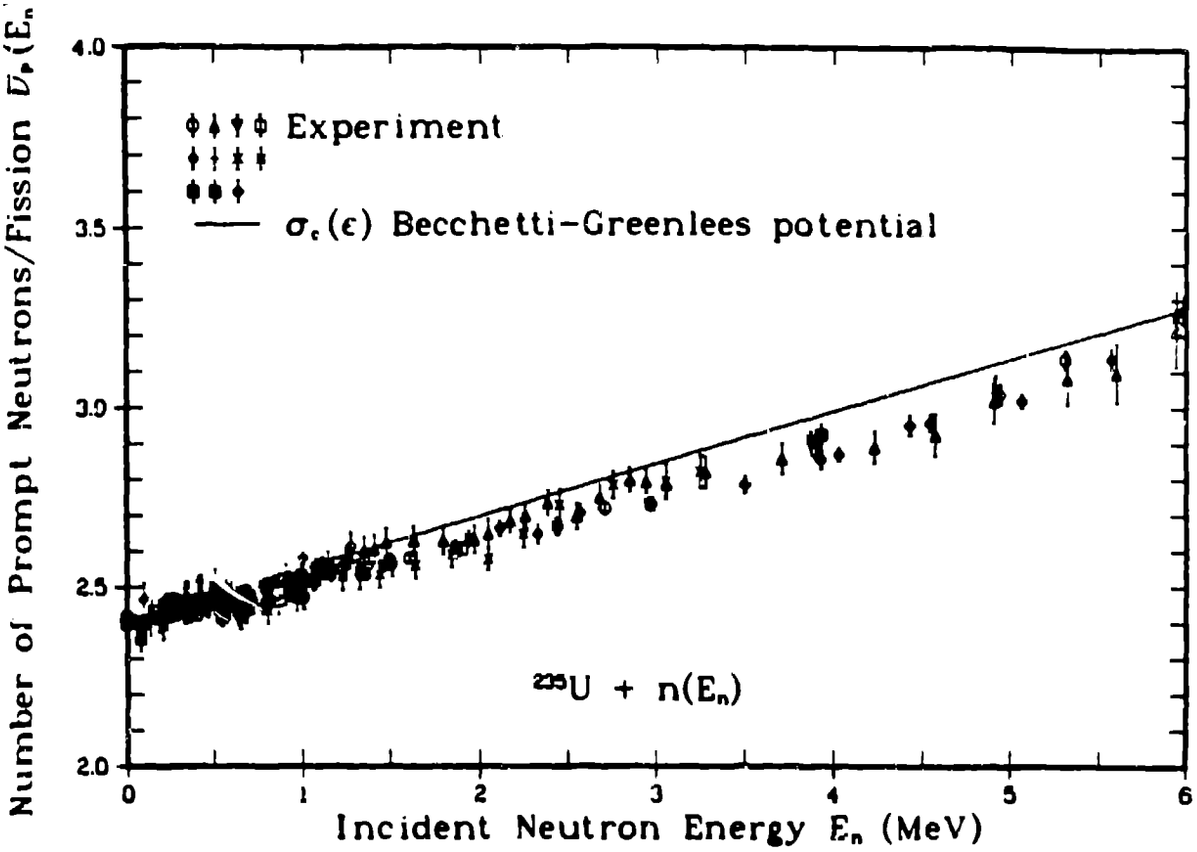
Number of Prompt Neutrons/Fission $\bar{\nu}_p(E_n)$
Experiment
$\sigma_c(\epsilon)$ Becchetti-Greenlees potential
$^{235}U + n(E_n)$
Incident Neutron Energy E_n (MeV)
4.0
3.5
3.0
2.5
2.0
0
1
2
3
4
5
6

Fig. 7.

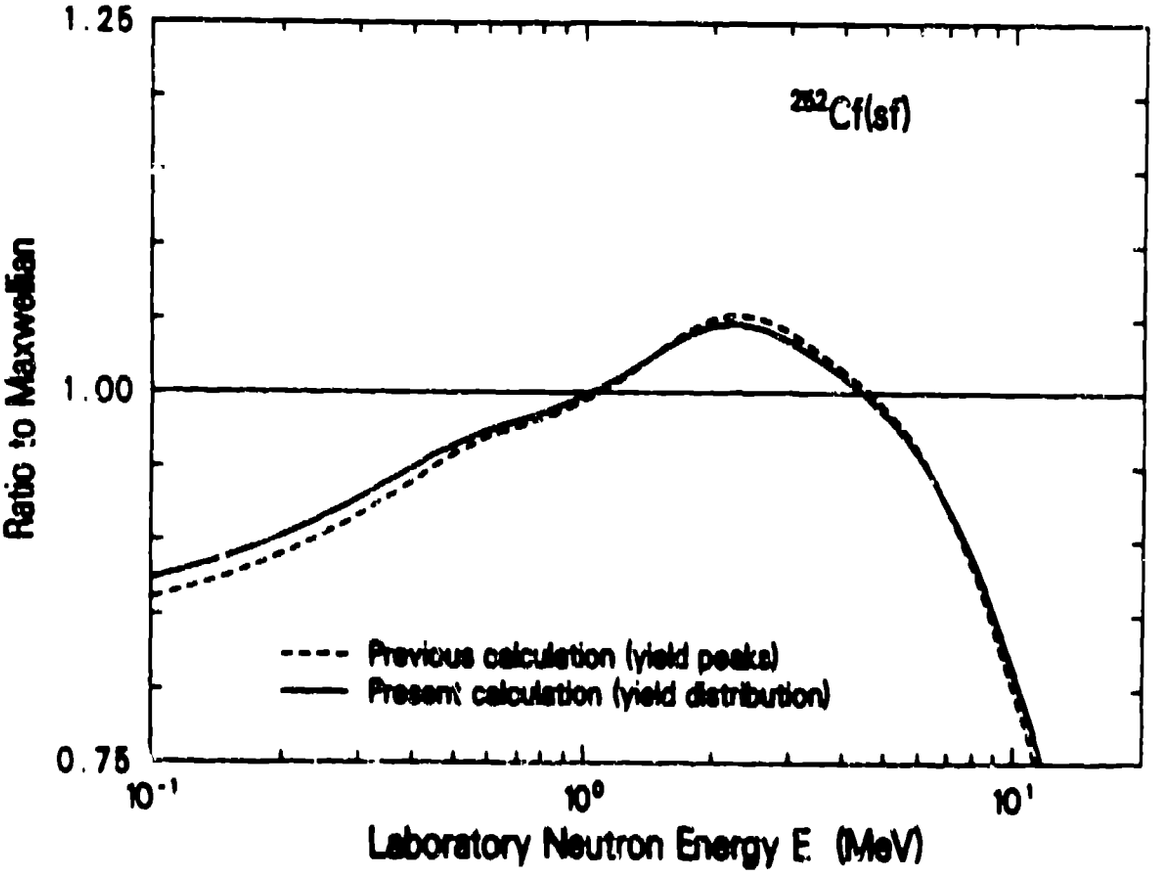
Ratio to Maxwellian
$^{252}Cf(sf)$
Previous calculation (yield peaks)
Present calculation (yield distribution)
Laboratory Neutron Energy E (MeV)
1.25
1.00
0.75
10^{-1}
10^{0}
10^{1}

Fig. 8.

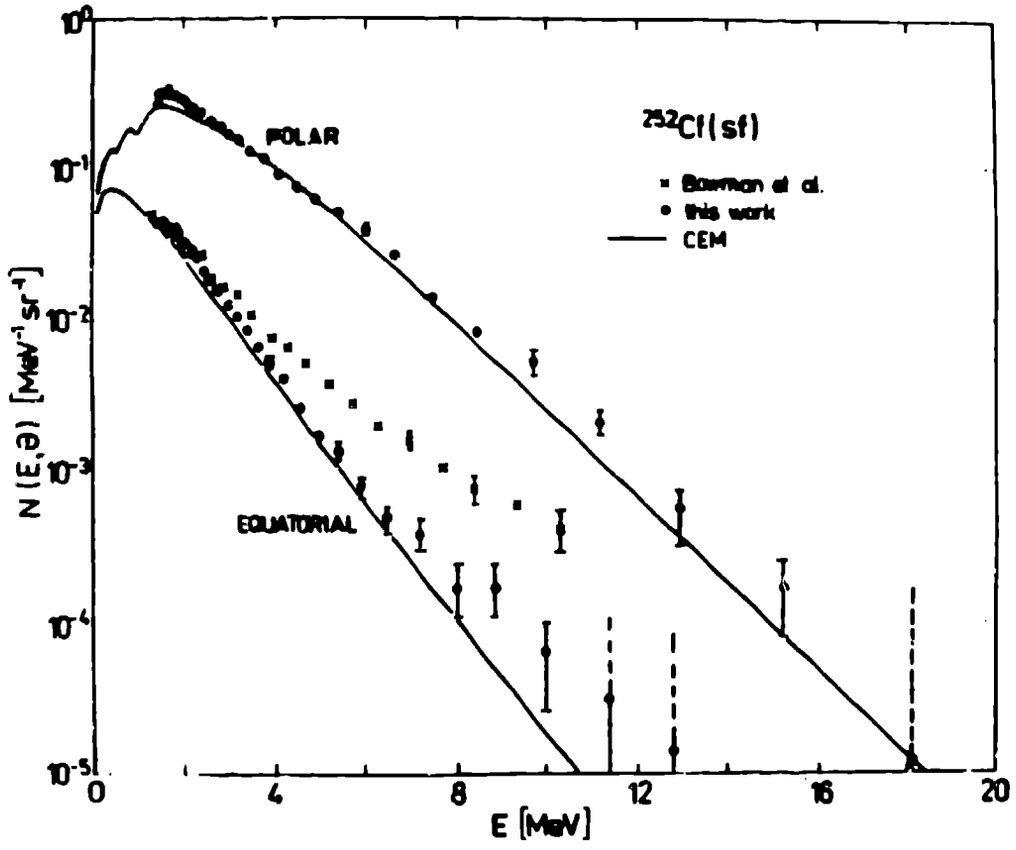
POLAR
EQUATORIAL
^{252}Cf(sf)
Bowman et al.
this work
CEM
N(E,ϑ) [MeV^{-1}sr^{-1}]
E [MeV]

Fig. 9.

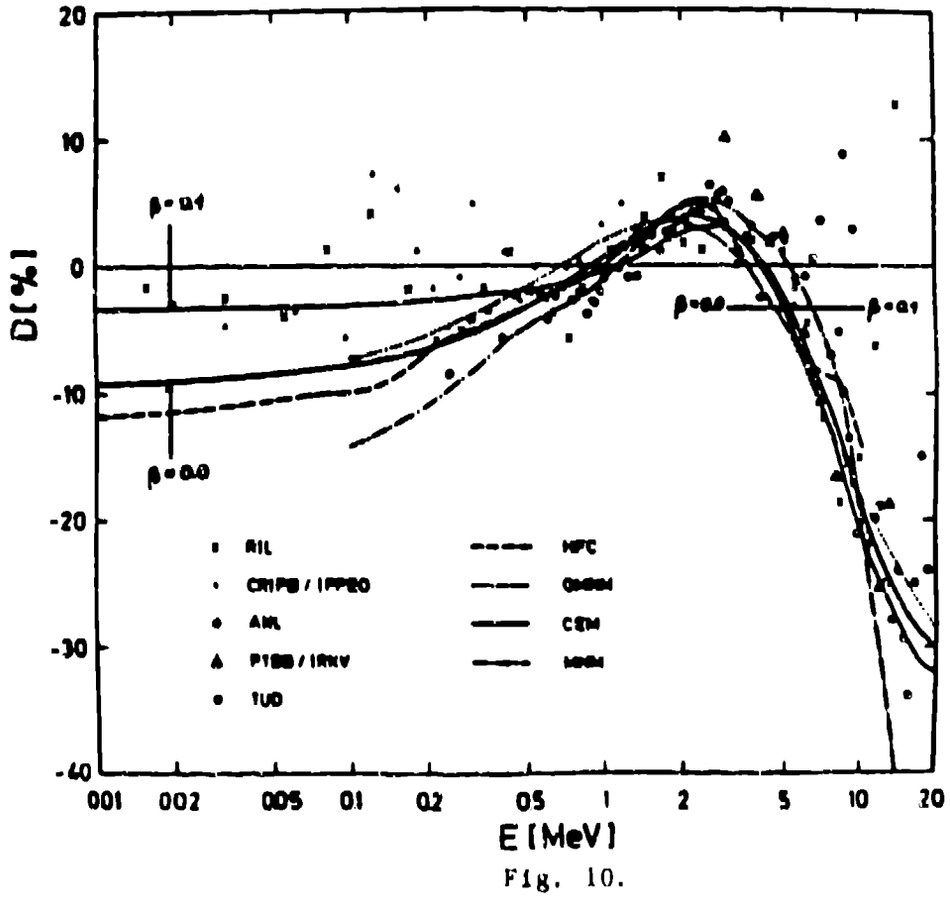
D[%]
E [MeV]
β = 0.1
β = 0.0
RIL
AML
TUD
CEM

Fig. 10.

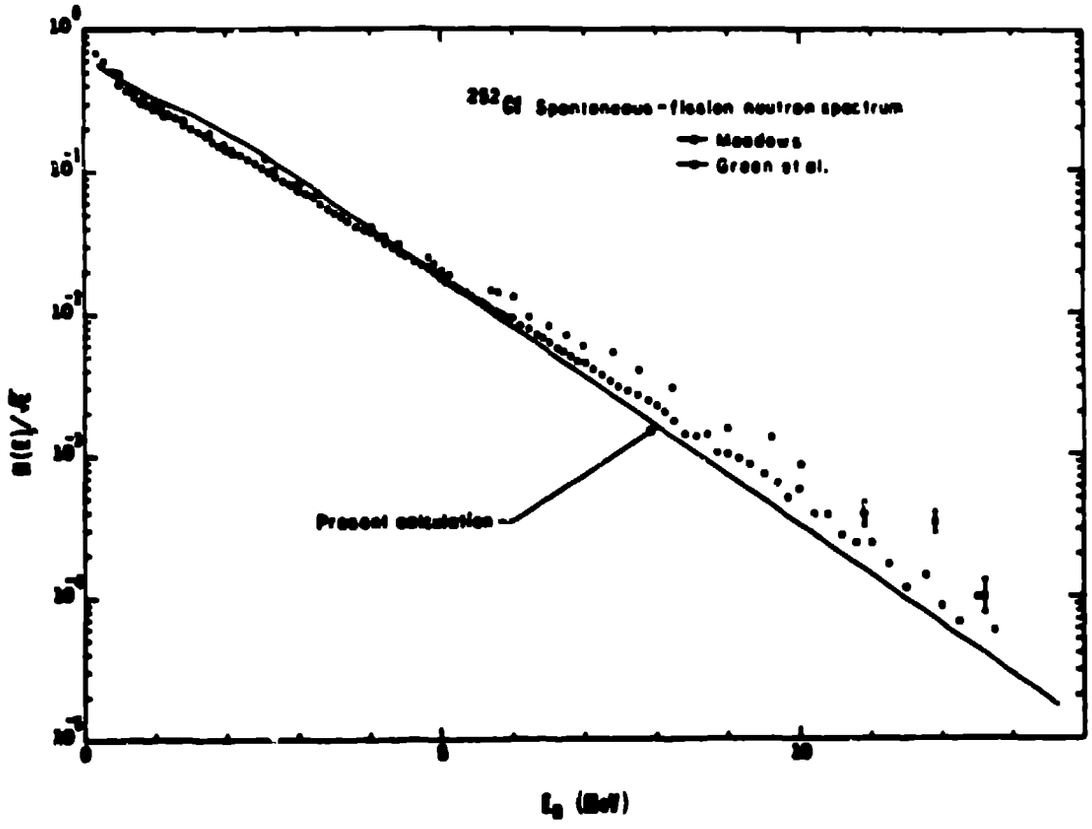
252Cf Spontaneous-fission neutron spectrum
Meadows
Green et al.
Present calculation

Fig. 11.

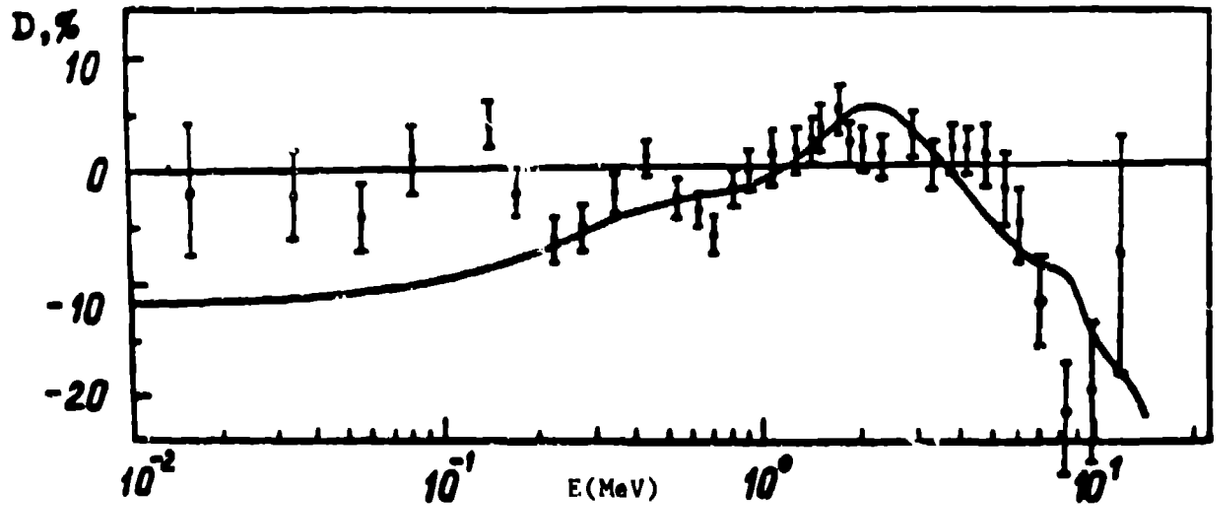
D,%
10
0
-10
-20
E(MeV)

Fig. 12.

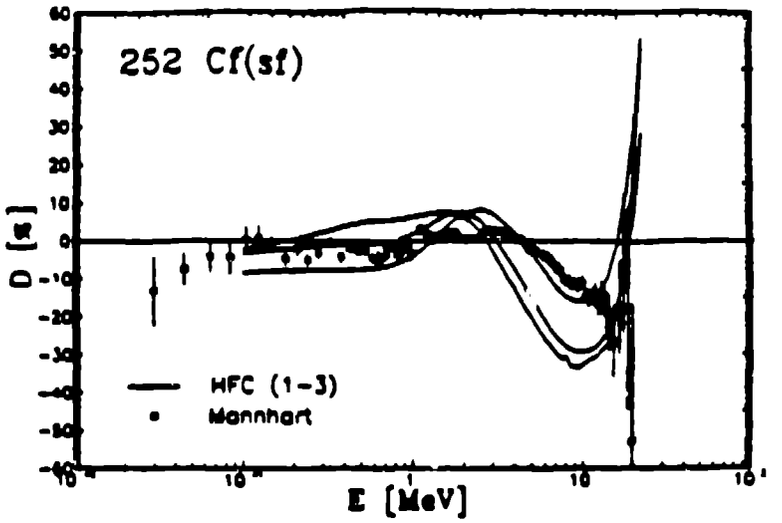
252 Cf(sf)
D [%]
HFC (1-3)
Mannhart
E [MeV]

Fig. 13.

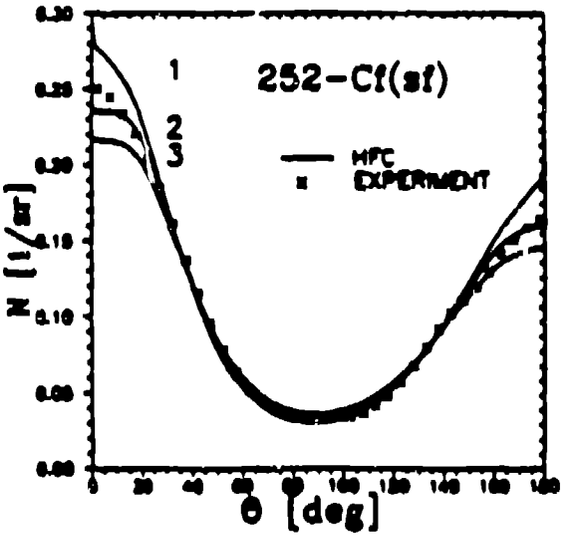
252-Cf(sf)
1
2
3
HFC
EXPERIMENT
N [1/sr]
θ [deg]

Fig. 14.

Fig. 15.

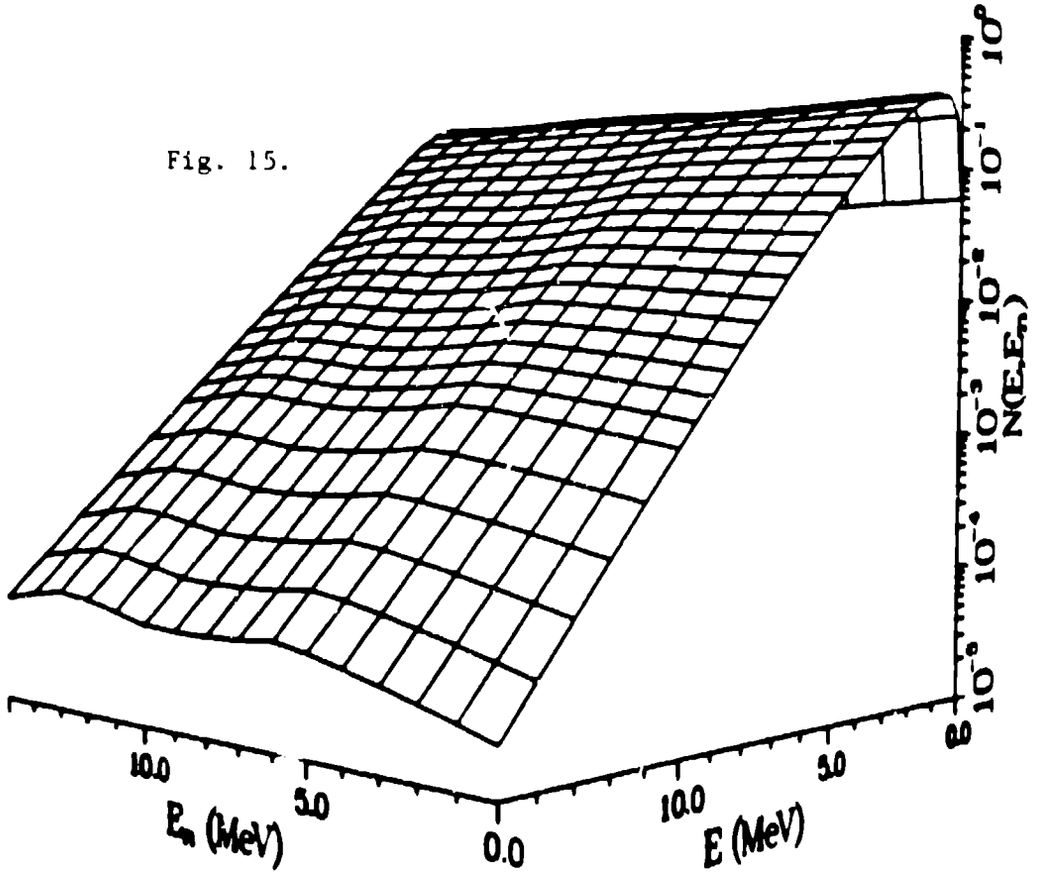
10.0
5.0
0.0
E_n (MeV)
10.0
5.0
0.0
E (MeV)
10^0
10^{-1}
10^{-2}
10^{-3}
10^{-4}
10^{-5}
N(E,E_n)

Fig. 16.

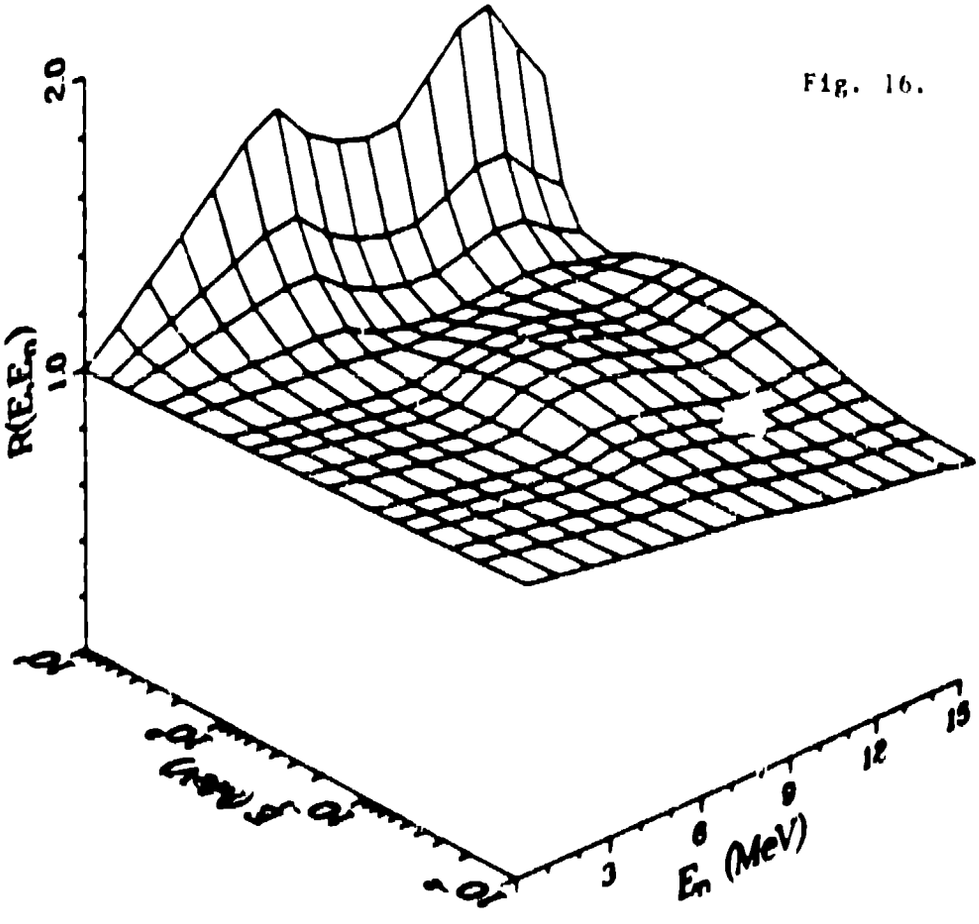
2.0
1.0
R(E,E_n)
3
6
9
12
15
E_n (MeV)

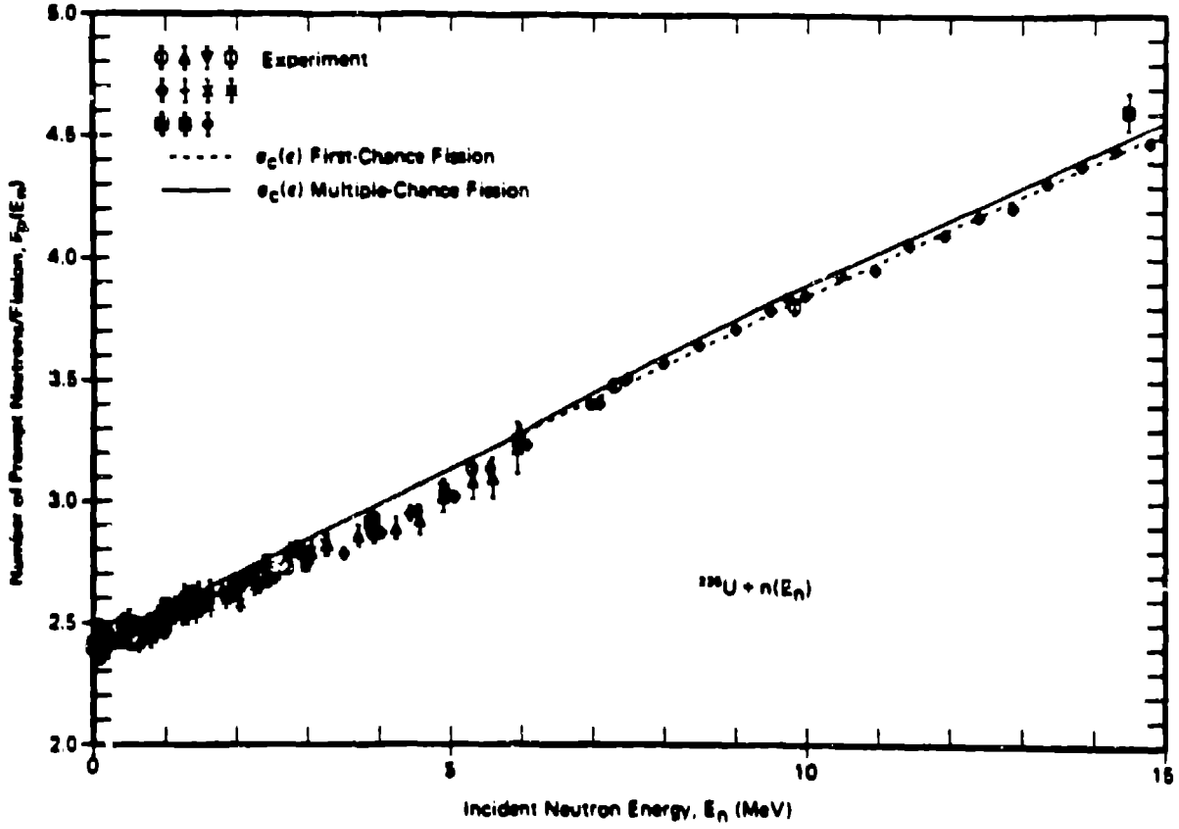
Experiment
$\sigma_c(\epsilon)$ First-Chance Fission
$\sigma_c(\epsilon)$ Multiple-Chance Fission
$^{235}U + n(E_n)$
Incident Neutron Energy, E_n (MeV)

Fig. 17.

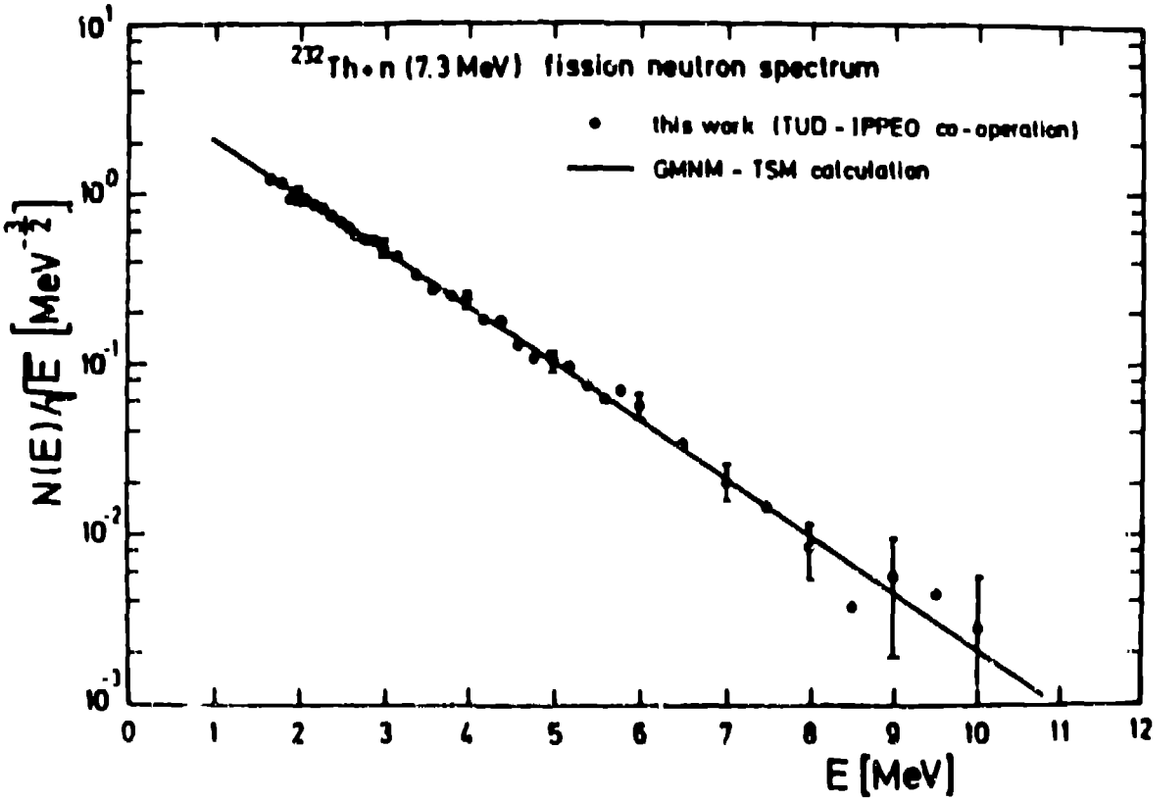
$^{232}Th + n$ (7.3 MeV) fission neutron spectrum
this work (TUD - IPPEO co-operation)
GMNM - TSM calculation
$N(E)\sqrt{E}$ [MeV$^{-\frac{1}{2}}$]
E [MeV]

Fig. 18.

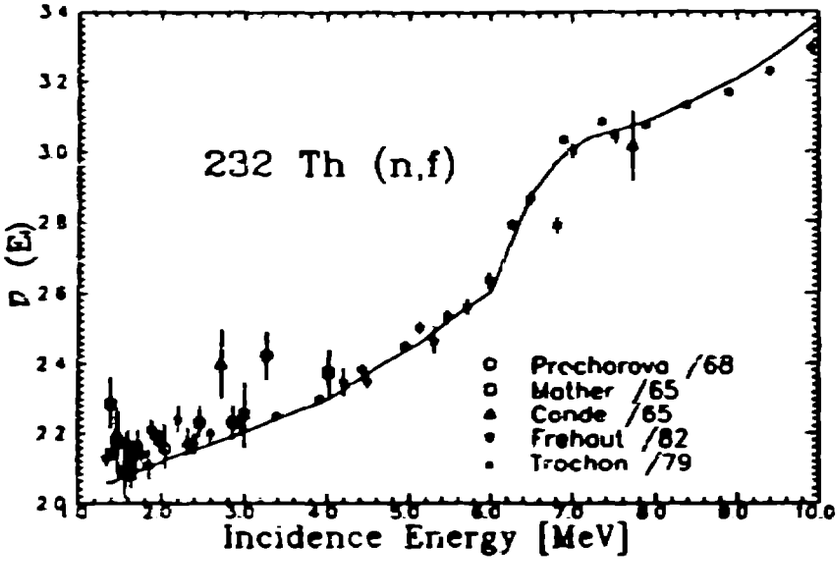
232 Th (n,f)
D (E)
Incidence Energy [MeV]
Prochorova /68
Mather /65
Conde /65
Frehaut /82
Trochon /79

Fig. 19.

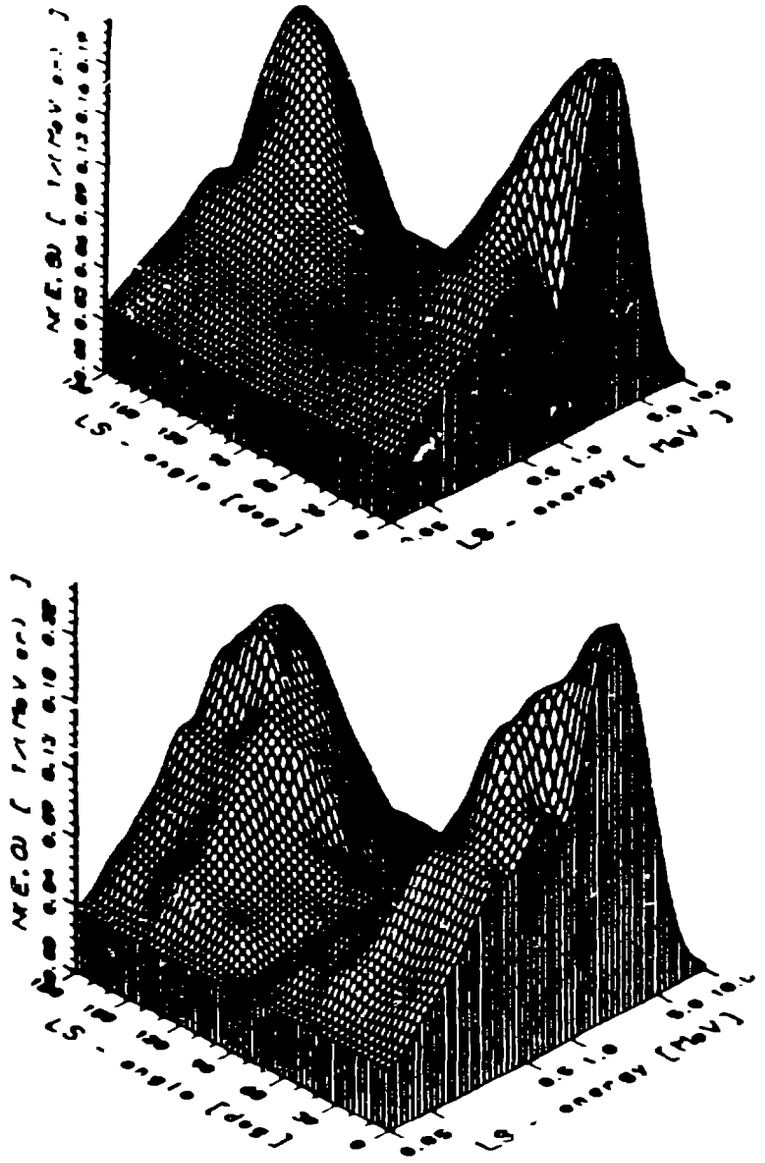

Fig. 20.

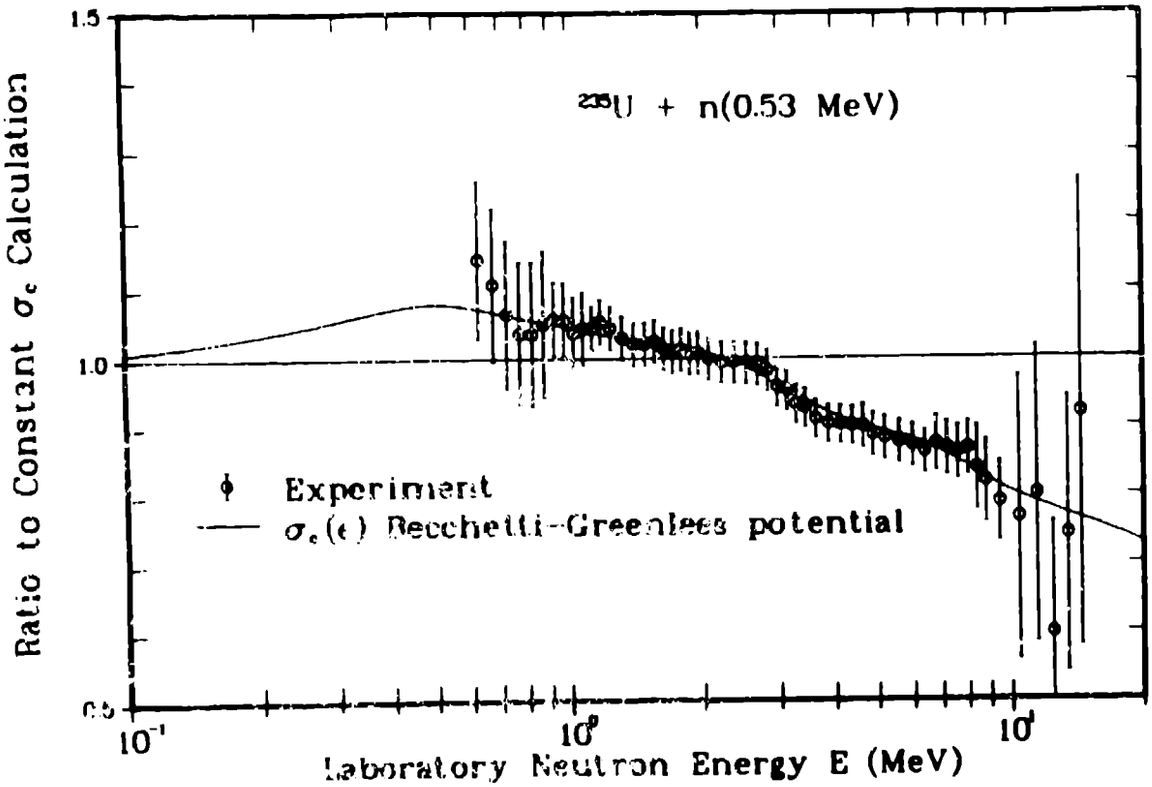

Fig. 21(a).

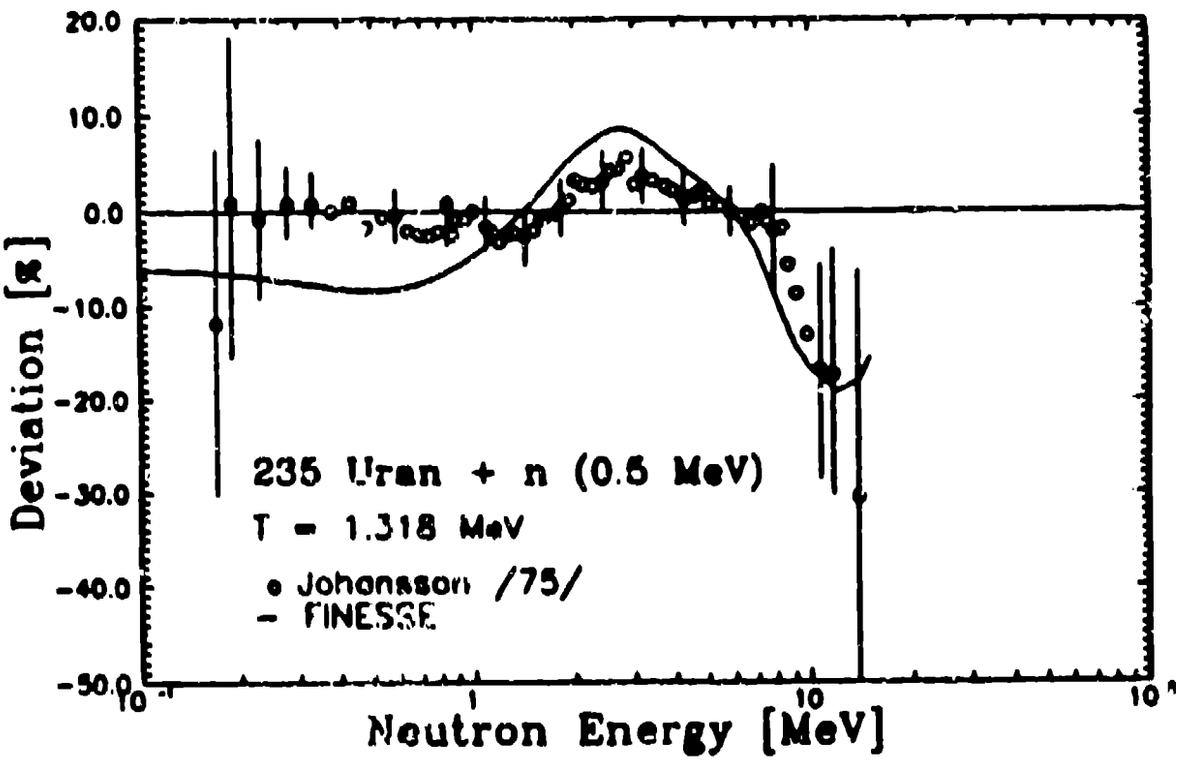

Fig. 21(b).

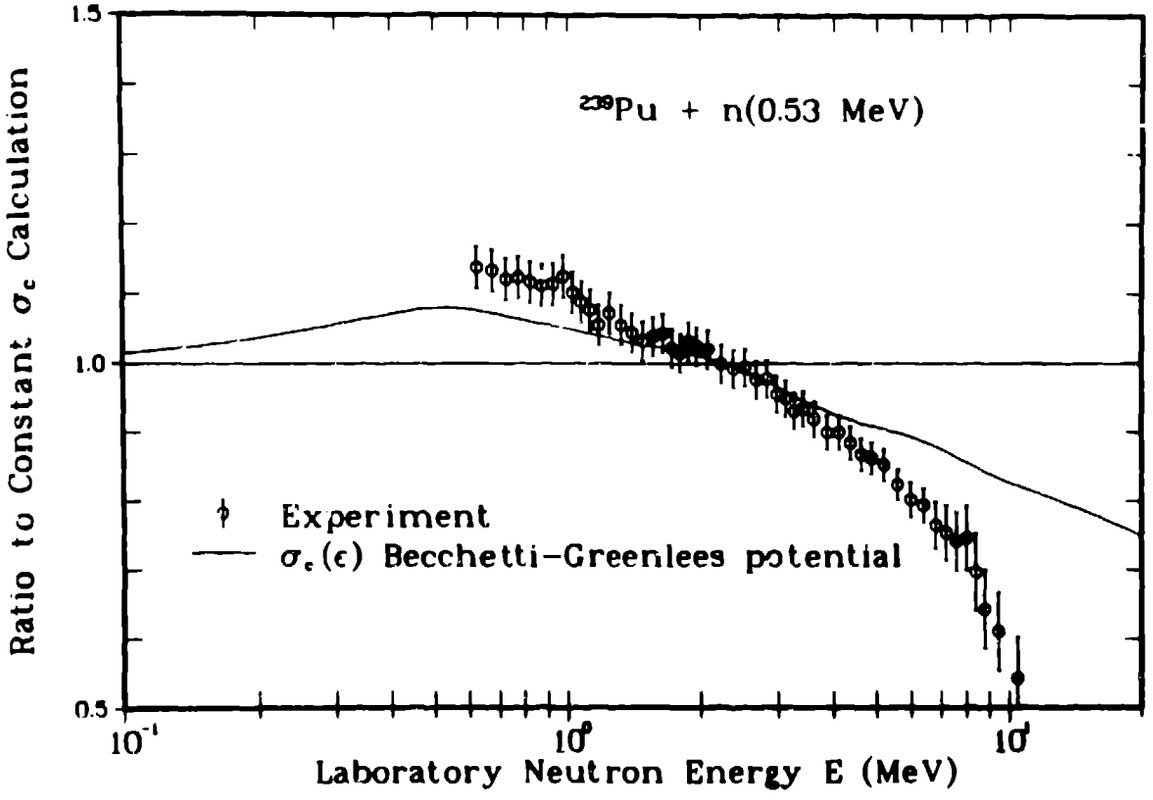

Fig. 22(a).

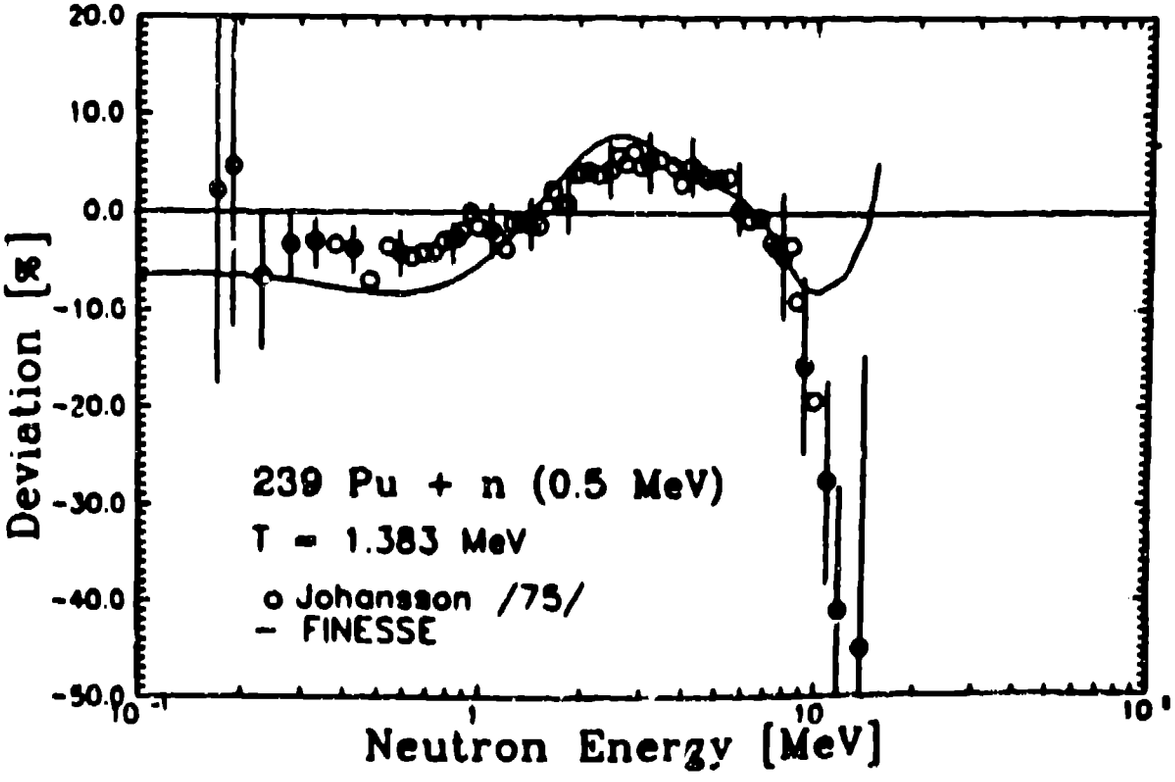

Fig. 22(b).

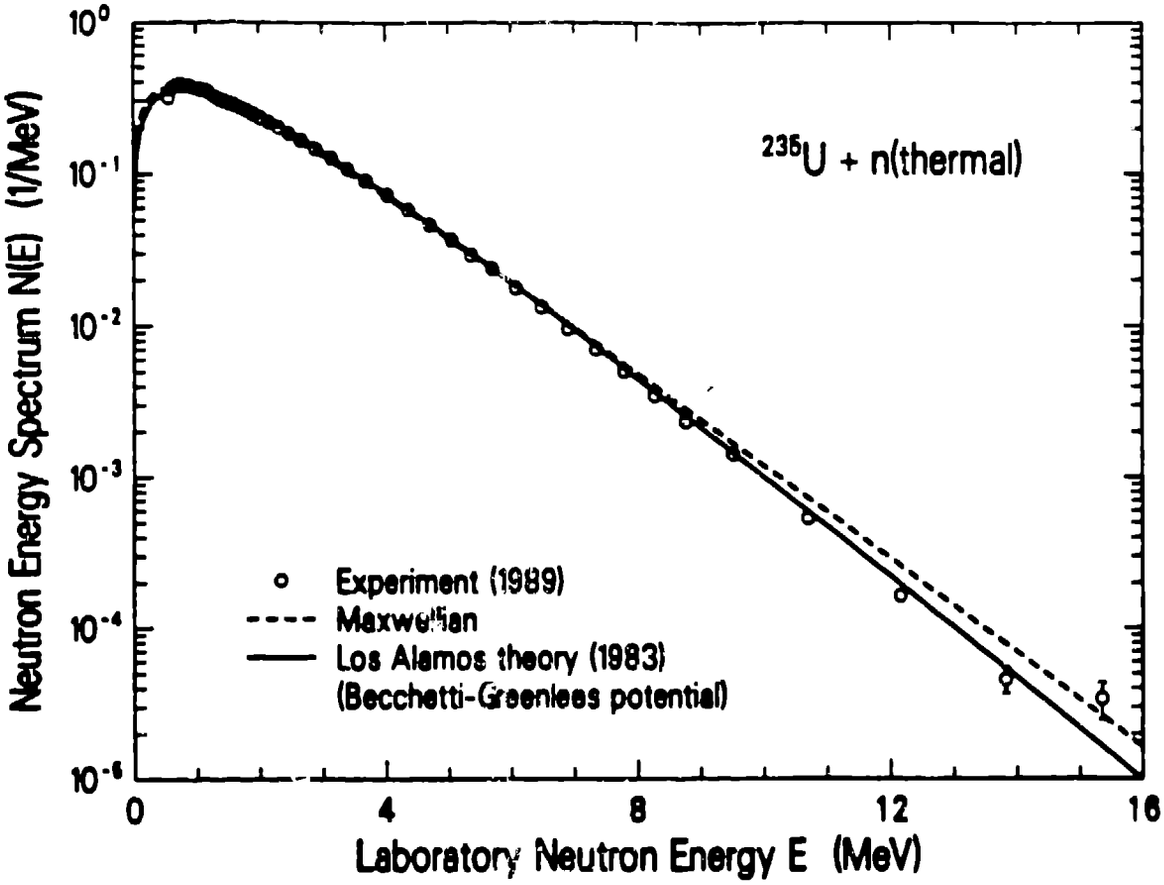
Neutron Energy Spectrum N(E) (1/MeV)
10^{0}
10^{-1}
10^{-2}
10^{-3}
10^{-4}
10^{-5}
^{235}U + n(thermal)
Experiment (1989)
Maxwellian
Los Alamos theory (1983)
(Becchetti-Greenlees potential)
0
4
8
12
16
Laboratory Neutron Energy E (MeV)

Fig. 23.

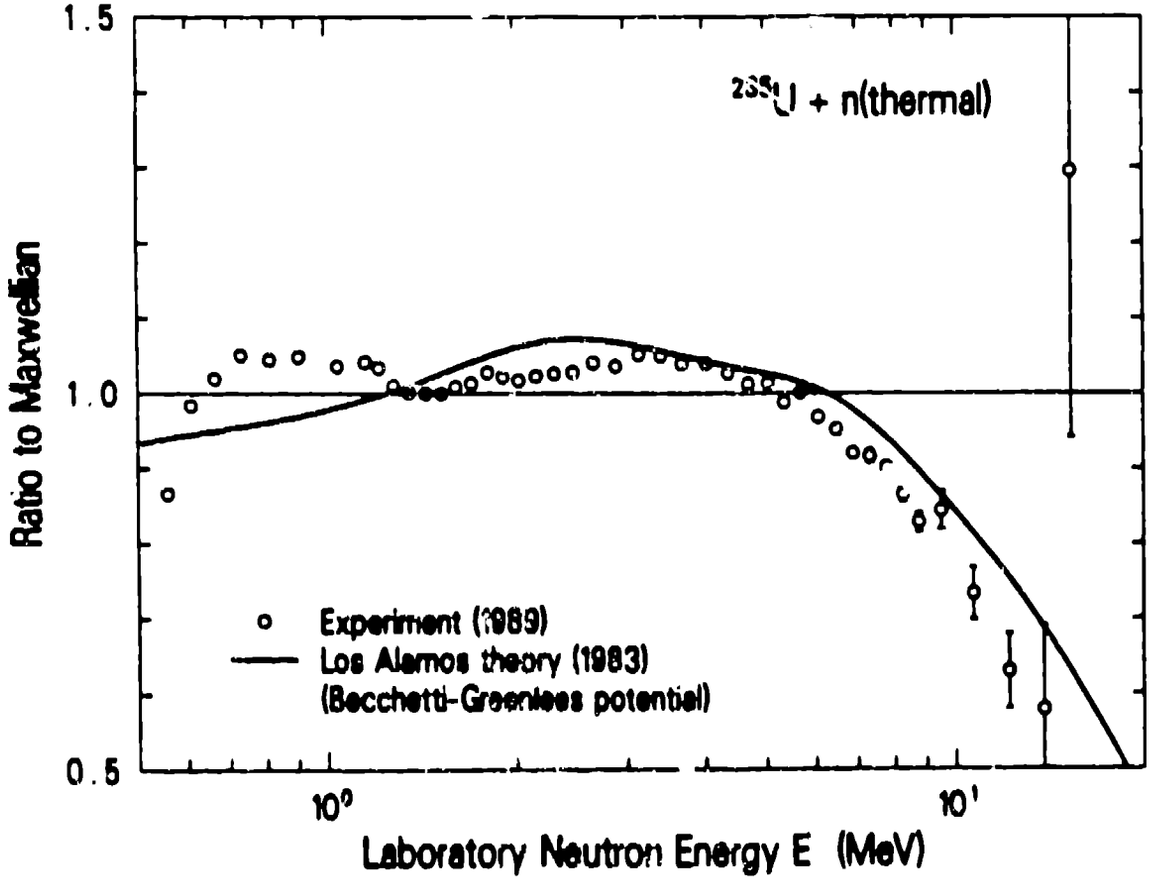
Ratio to Maxwellian
1.5
1.0
0.5
^{235}U + n(thermal)
Experiment (1989)
Los Alamos theory (1983)
(Becchetti-Greenlees potential)
10^{0}
10^{1}
Laboratory Neutron Energy E (MeV)

Fig. 24.

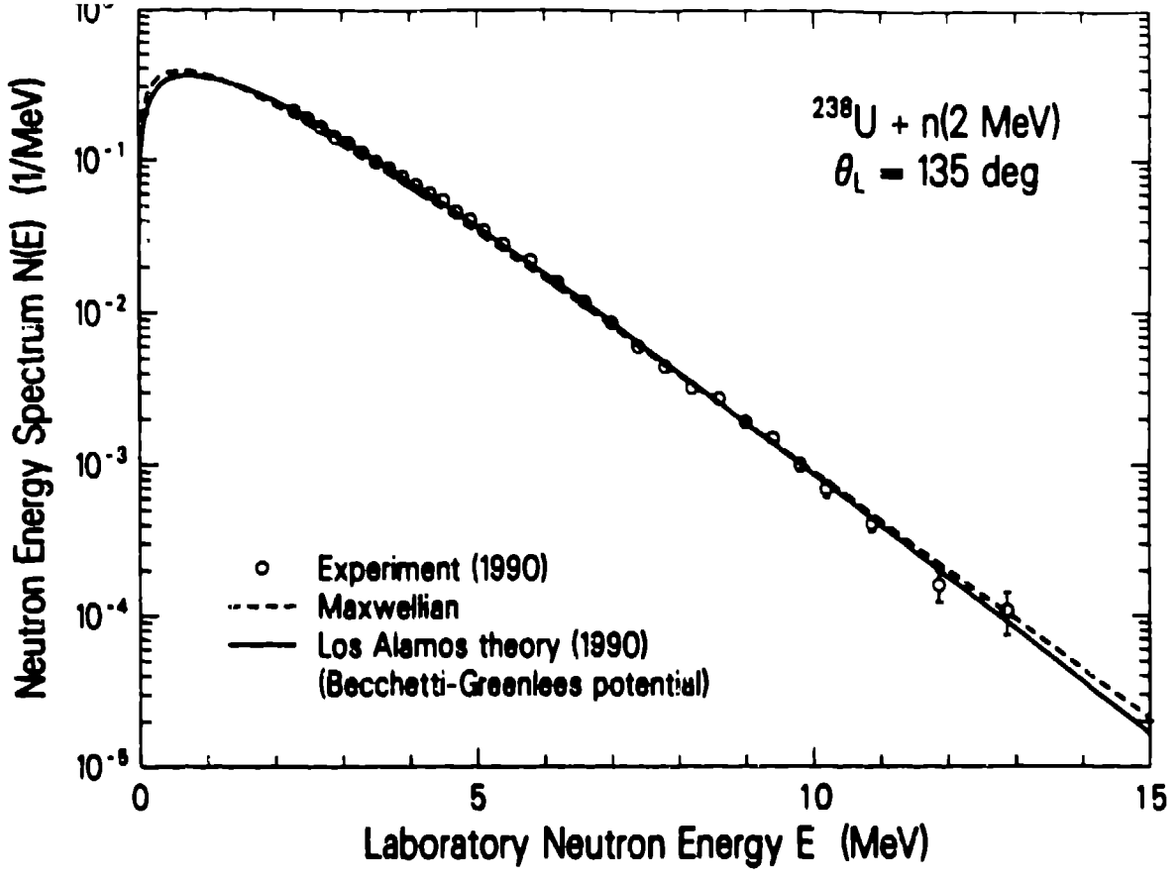
^{238}U + n(2 MeV)
θ_L = 135 deg
Experiment (1990)
Maxwellian
Los Alamos theory (1990)
(Becchetti-Greenlees potential)
Neutron Energy Spectrum N(E) (1/MeV)
Laboratory Neutron Energy E (MeV)

Fig. 25.

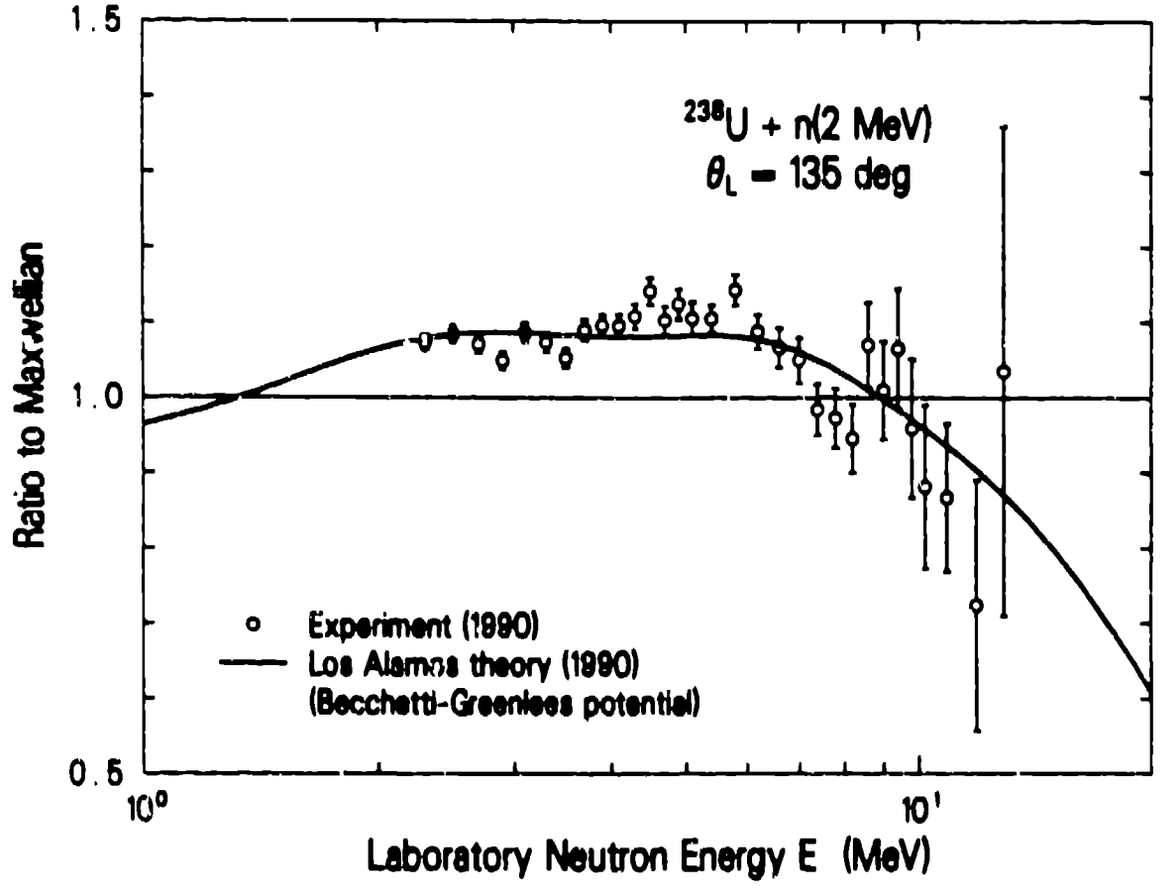
^{238}U + n(2 MeV)
θ_L = 135 deg
Experiment (1990)
Los Alamos theory (1990)
(Becchetti-Greenlees potential)
Ratio to Maxwellian
Laboratory Neutron Energy E (MeV)

Fig. 26.